The Dynamics of a Binary Granular Mixture in a Rotating Tube

by

Kiam Choo

A thesis submitted in conformity with the requirements

for the degree of Master of Science

Department of Physics

University of Toronto

Abstract

For this thesis, we studied the dynamics of a binary granular mixture in a rotating tube. Like previous workers, we observed the formation of bands due to the segregation of the two species, as well as the merging and splitting of the bands. In addition, we observed linear travelling waves. We measured the dispersion relation of the travelling waves, and also the velocity dependence on the mixture ratio. The waves stop travelling above a wavelength cutoff and below a mixture ratio cutoff. Near the cutoffs, the travelling waves lose linearity and merge rather than pass through each other. Travelling pulses, sources and possibly sinks were also observed. These results invalidate previous theories on the system. From Fourier analysis of the segregation effect, we were able to determine that the system experiences wavelength selection that is independent of rotation rate, and that the growth in structure varies with rotation rate, and has a peak at about $\omega = 4$ Hz.

Acknowledgements

I thank my supervisor, Professor Stephen Morris, for his advice and insights. I also thank Tim Molteno for technical advice, and Michael Baker for providing some recent results on this project. Past efforts by Eamonn McKernan, Elaine Lau and Holly Cummins on prototype experiments are also much appreciated. Last but not least, many thanks go to Wayne Tokaruk and Zahir Daya for advice and stimulating discussions on Friday afternoons.

Contents

List of Figures

I. INTRODUCTION

In 1939, the Japanese scientist Y. Oyama noticed that a binary mixture of large and small-grained sand segregated into bands (as shown in Figure 1) when rotated in a tube in such a way that the sand streamed smoothly [1]. This constituted the first observation of axial segregation in the system studied in this thesis: a binary granular mixture in a rotating tube.

This segregation effect is counterintuitive because the churning motion of the tube's rotation would seem to have a mixing rather than an ordering effect. So, after a hiatus of several decades, this system has captured the imagination of many researchers, and work on it has recently resumed in earnest [11–15,17,18]. Oyama's original experiment used a binary mixture of sand, but the effect has been reproduced in glass beads and a mixture of rice and peas as well, showing that it is robust under change of material.

In a typical experiment in this rotating tube system, equal amounts of the two grain species are uniformly mixed and then put into the tube. The tube is then rotated horizontally about its long axis. The bands first appear after a few tens of rotations. They are visible because the two grain species are usually chosen to have contrasting colours. The bands are faint at first, but intensify.

It has been found that the bands that form in the tube may merge or sometimes split, with a tendency towards merging [6,13,15]. Merging and splitting events are comparatively rare.

Workers have also found that the occurrence of axial segregation seems to require that the dynamic angle of repose (i.e., the angle of the flowing surface) be different for the two species [13,18]. This has been taken to be evidence that surface flows are responsible for the segregation, and has inspired a theoretical model [17] that derives the segregation as diffusion with a negative coefficient.

Some workers have also studied the number of bands that appear. It is claimed that more bands appear when more small particles are used [13], and that more bands appear

when the rotation rate is slowed [15]. Recently, however, MRI studies have shown that there exist subsurface bands that may not be visible from the surface [19]. This suggests that visual band counting may be missing some bands.

Spatially periodic structures have often been observed in other systems, known as pattern forming systems. The presence of periodic bands in the rotating tube suggests that it is a pattern forming system as well.

A. Pattern formation

When driven externally, spatially extended dissipative systems may spontaneously break translational symmetry and evolve periodic patterns. This *nonequilibrium pattern formation* has been the subject of considerable study lately [2]. It is interesting and important because periodic patterns are ubiquitous in nature, and include sand ripples, snowflakes, flame fronts and even stripes on a zebra. Below we describe two examples of pattern formation in fluids.

Rayleigh-Benard convection is the classic example of pattern formation. When a fluid is placed between two horizontal parallel plates, and it is heated from below, an unstable situation develops in which the bottom fluid is less dense than the top. This is the *instability* that tends to cause a bulk overturning of the fluid with a length scale similar to the plate separation. When this overturning is realized, convection is formed. But because of opposition from viscous forces, convection does not occur until the Rayleigh number, which is the ratio of the destabilizing buoyancy force to the stabilizing viscous force, reaches about 1708. This number is independent of the fluid. From above, these convection cells appear as parallel rolls. Under different fluid properties, hexagons and squares may be observed.

The Faraday instability is another fluid pattern forming system. Like Rayleigh-Benard convection, it also forms rolls, squares and hexagons. However, it forms patterns on a free upper surface, and instead of being heated, it is driven by vertical vibration at some frequency f. Above a certain critical acceleration amplitude, an instability occurs that typically shows squares at onset. The patterns that result oscillate at a frequency of precisely

$f/2$.

Because Oyama's axial segregation evolves periodic patterns, it appears to be an example of pattern formation as well. However, the source of its instability is not known.

There is a whole field of *equilibrium* pattern formation as well, but for simplicity, pattern formation will henceforth in this thesis refer only to the nonequilibrium case.

B. Pattern formation in granular matter

Granular matter encompasses a large class of materials including sand, soil, food products, pharmaceutical pills, and even hair. Granular matter has attracted a great deal of interest in recent years due not only to its industrial importance [4], but also to its unusual properties [5].

At first sight, one might think that granular matter might behave like fluids because it can flow like a fluid. Closer study indicates otherwise. For instance, granular matter needs to expand in order to undergo shear: at rest, the grains are tightly packed, so that for shear to occur, the spacing between grains must increase. Also, large objects tend to float in granular matter, even if they are denser than the surrounding material. An amusing demonstration of this effect is as follows: if one puts a steel bolt at the bottom of a container, then fill it with sand, the bolt will rise to the top when the container is vertically vibrated. This effect occurs even though the bolt is denser than the sand, and stands in stark contrast to the buoyancy behaviour of liquids. This effect has been found to be due to the creation of convection rolls that travel down at the container walls, and up in the centre. Thus, the bolt gets carried up by the current in the centre, and once on top, is too large to follow the sand down the sides of the container [10].

Some of granular matter's unusual behaviours include a rich variety of pattern forming behaviour. The patterns formed often resemble fluid patterns. We describe a few of them here.

Granular matter can exhibit convection rolls that strongly resemble Rayleigh-Benard

convection. Aoki *et al.* [24] have explored granular convection in a vertically-vibrated rectangular cell. Unlike Rayleigh-Benard convection, the driving is vibrational rather than thermal, and the granular matter is not constrained between a pair of upper and lower plates, but has a free upper surface. Also that this is not like the Faraday instability as convection rolls form, not surface waves. Above a critical acceleration amplitude Γ, a pair of convection rolls form at opposite ends of the cell. These rolls flow downwards along the edges of the container. These convection rolls are likely to be the same ones that cause the steel bolt to rise in the example mentioned previously. If Γ is increased, one finds a transition to rolls that flow *upwards* along the edges of the cell. This mode of convection is more stable, and can result in multiple roll pairs: Aoki *et al.* have observed up to 8 rolls. The number of rolls seen depends primarily on the aspect ratio (i.e., the width divided by the height) of the cell. The critical acceleration amplitudes are not strongly dependent on the vibrational frequency.

Periodic wave-like structures have also been observed in a vertically-vibrated cell containing lead particles [8]. The system is several layers high and one particle deep. The system is driven sinusoidally. When the acceleration amplitude Γ reaches a critical value, the layer becomes unstable to periodic wave-like structures. This appears to be the one-dimensional analog of the two-dimensional patterns seen in the experiments of Umbanhower *et al.* [23], which strongly resemble those seen in the Faraday instability. In Umbanhower's granular system, a vertically-vibrated bed exhibits rolls, hexagons, squares, and oscillons under different driving. The latter is a long-lived, localized spatial structure that appears as a peak on one oscillation, then a crater on the next. Oscillons are particularly interesting as they can bond to form 'molecules' and even 'crystals'. The transitions from one form of pattern to another as Γ is varied has been successfully modeled by bifurcations in the flight time of a single completely inelastic ball driven by an oscillating plate [23].

C. Motivation

The striking similarities between fluid patterns and granular patterns occur despite the fact that the properties of granular matter are quite different from those of fluids, and the conditions under which the patterns are generated are often different. For instance, the vibrated-bed patterns can be simulated in a very un-fluidlike manner using ballistic motion and particle-particle inelastic collisions [9]. Clearly, the underlying physics of the granular system is quite different from that of the Faraday instability, and this provides strong motivation for studying pattern formation in granular matter.

There is also the motivation of increasing our understanding of granular matter. Interest in granular matter in the physics community has bloomed in recent years. The attractions are manyfold. They include: the richness of the behaviour of granular matter [5]; the opportunity to study a completely new form of matter whose constituent particles interact dissipatively; the potential to generalize results from granular physics to other dissipative systems; and the possibility of applying theories from other fields like traffic flow [20]. Despite the best efforts of many people, the field is still in an early stage of development, and our understanding of it is still very shallow.

So from the granular physics standpoint, this system represents another unusual phenomenon that begs to be explained by some future theory of granular matter, and the elucidation of the properties of this system will serve not only as a testbed for such a theory, but may well aid in its development.

Finally, the existence of opportunity is a motivating factor as well. While many groups have studied the rotating tube system, hardly anyone has subjected it to the rigorous scrutiny of computerized data capture and analysis. Indeed, most work has been very qualitative to date. Thus, there was the opportunity to observe undiscovered dynamics by using the right tools to examine the system in detail.

D. Outline of this thesis

In this project, we studied the dynamics of a mixture of sand and salt in a pyrex tube. The primary improvements we made over previous efforts were in the video capture and analysis, as well as the much larger aspect ratio of the tube we used.

We define the aspect ratio of the tube to be the length of the tube divided by its diameter. Two tubes of the same diameter were used in the results reported in this thesis. Their aspect ratios are 40.6 ± 0.2 and 38.6 ± 0.2. These large aspect ratios (~ 40) are a novel feature of this experiment. By employing a large aspect ratio, a larger number of bands can be studied, yielding Fourier peaks that are well separated from DC and have good resolution.

We captured images of the flowing surface using a computer-controlled video camera. By composing a spacetime evolution diagram of the surface colour, we were able to discern travelling waves and other structures. In this thesis, we characterize the travelling waves' speeds as a function of wavelength and relative proportions of the two granular species. We also report on transitions from travelling waves to stationary waves.

Segregation was also studied in Fourier space. We identify the growth of the bands with the growth of Fourier modes, and define a parameter that allows us to identify the point in time when the sand bands become saturated with sand. We show that the rate at which the bands grow depend on the tube's rotation rate. We also show that our system experiences wavelength selection.

Finally, we comment on the connection between our work and that of others', and we suggest that the system exhibits behaviour similar to that of other pattern forming systems. We outline some constraints placed by our results on theoretical models, and discuss possible phenomenological and physical theories. We conclude with a discussion of future work.

E. Apparatus and Method

In this chapter, we describe in detail the apparatus that we used, as well as the data analysis procedure.

F. Apparatus

The apparatus consists primarily of a pyrex tube roughly one third filled with a mixture of black sand and white table salt. The tube was rotated about its long axis at a constant angular frequency using a computer-controlled stepper motor. Figure 1 in the Introduction shows the setup schematically. Two tubes were used in this thesis. They were $\sim$1 m long, with inner diameter 27 mm. Their aspect ratios are 40.6 ± 0.2 and 38.6 ± 0.2. The tubes were bounded by teflon-covered plugs.

As the tube rotates, the sand/salt mixture organizes into bands as shown in Figure 1. The surface brightness of the flowing material was visualized using a monochrome CCD video camera, on which was mounted a wide angle lens (Cosmicar C60305, focal length 3.7 mm) that can image the entire length of the tube.

The whole setup was enclosed in a styrofoam housing in order to control the lighting. Lighting was provided inside the housing by a single fluorescent tube running parallel to and above the pyrex tube. Due to limitations on the size of the housing, the camera had to be situated outside. The camera imaged the tube through a small slot that had a negligible influence on the lighting conditions inside the housing.

The video signal captured by the camera was fed into a computer via a frame grabber card (Analogic FG/ALU-8). Analysis occurred offline, and was done in Fourier space. Details are given later in the section on Analysis.

The humidity of the enclosure housing the experiment was monitored with a hygrometer, and was found to vary from 18 - 34%. In earlier experiments, sticking due to static charging was noticed to appear to enhance segregation. As humidity was thought to influence the

degree of static charging present in the system, it was monitored. However, the experiments reported in this thesis were not observed to have any significant sticking.

G. Samples

The sand used was black hobby sand [27], while the salt used was Sifto salt commonly obtainable in convenience stores in Toronto.

Under a microscope, it can be seen that most salt particles have a cubic crystalline shape. A small fraction are irregularly shaped. The black sand, on the other hand, are all fairly irregularly shaped, and have the general appearance of little boulders.

Two different types of mixtures were used for the experiments. The size distributions of the sand and salt components in each type of mixture are shown in Figure 2. The sand used was smaller than the salt in both cases. Mixture B has a larger variety of particle sizes, and has smaller sand particles on average than Mixture A.

We define the *mixture ratio* ϕ to be the volume fraction of salt in a mixture. Type A was fixed at a mixture ratio of 50%, while Type B's mixture ratio was varied between 33% and 77%.

H. Method

For separating out various-sized particles, 5" standard sieves were used. Various sieve cuts were obtained by manual shaking in a horizontal plane. Care was taken to ensure that the shaking was done in a reproducible way.

The tube was filled by first placing the sand/salt mixture in a U-shaped aluminum channel, then inserting it lengthwise into the tube, and then dumping its contents. Two such fillings were used for each run. Dividing the total volume of material put into the tube by the volume of the tube, one gets that $28 \pm 2\%$ of the tube is filled. This number is an indication of the filling fraction only; it does not mean that 28% of the tube is filled, as the packing of the grains changes when dumped into the tube. The exact filling fraction

is also changed by rotation and by segregation. The reason is that packing effects depend on the mixture ratio, while the angular velocity determines the shear rate, which in turn determines the volume of the material, since granular matter expands under shear.

Many of our experiments utilized a uniformly mixed initial state for the sand/salt mixture. These are called *premixed runs*. Like many other granular materials, the sand and the salt have a tendency to segregate despite one's best attempts to mix them together. As a result of this tendency to unmix, a perfectly uniform initial state cannot be achieved. Typically, a 'uniform' initial state that has been prepared to the best of the experimenter's ability will still contain some concentration fluctuations that are visible to the naked eye.

Many of our experiments also used non-uniform initial states. These presegregated initial states were obtained by placing partitions in the U channel and then filling each segment with the desired mixture. These are called *presegregated runs*.

I. Analysis

Data received from the camera was stored on computer as images files that were composed of stacked frames captured at regular time intervals. Each frame consisted only of a long rectangle containing an image of the flowing surface. Such spacetime plots were useful for visualizing the time evolution of the bands. Analysis was also conducted in Fourier space. This section describes the procedure used to obtain the Fourier spectra.

J. Image Division

The images were stored as 8-bit TIFF files, then converted to a binary file that encodes an array of floating point numbers for analysis.

Representing the data as floating point numbers is essential for analysis as information would in general be lost if the results of an operation on an 8-bit TIFF image were shoehorned back into an 8-bit TIFF. For instance, if two 8-bit TIFF files are multiplied, each pixel in the resulting image has 16 bits of information.

The first step in the image analysis is to divide out the spatial intensity variations introduced by the lighting. That is, we wish to analyze:

$$\frac{I(x,y)}{I_0(x,y)} \tag{1}$$

where $I(x,y)$ is the intensity imaged at position (x,y), and $I_0(x,y)$ is the flat frame intensity at the same position. The flat frame is the image obtained by capturing a uniformly coloured surface at the same position and under the same lighting conditions as that used to capture $I(x,y)$.

The grey levels captured by the frame grabber card are linearly related to intensity. Thus, if the grey level at position (x,y) is given by $G(x,y)$, then:

$$G(x,y) = aI(x,y) + D(x,y) \tag{2}$$

where $D(x,y)$ is the grey level registered at (x,y) by the frame grabber when there is zero intensity there. $D(x,y)$ is obtained by imaging a frame with a cap over the camera lens.

Using 1 and 2, we see that the data we want to analyze is given by:

$$\frac{G(x,y) - D(x,y)}{G_0(x,y) - D(x,y)} \tag{3}$$

where $G_0(x,y)$ is the grey level at (x,y) for a flat frame.

K. Image Undistortion

The next step is undistortion. Because of the length of the tube, it was necessary to use a very wide angle lens, which has significant distortion. The nature of the distortion may be seen in Figure 3. Clearly, the outer areas of the image are compressed, which can cause errors in distances measured there if left uncorrected. As the wavelengths of the emergent bands are of interest, it was necessary to correct for the distortion. Figure 4 shows the grid after a correction is applied. The correction is not perfect at the corners of the field of view, but it is very good along the horizontal centre of the image, which is all we need, as we capture images of the tube only from a long horizontal rectangle near the centre.

The undistortion function can be derived by considering a simple ray optics model of the camera lens. We assume that the lens focuses its image on to the surface of a sphere instead of a plane. As the CCD is a plane, the distortion results from the nonlinear projection of a point on a circle on to a nearby line, as shown in Figure 5. We assume that the distortion is azimuthally symmetric. Thus, in the figure, x and X represent radial distances from the axis of the lens.

The mapping from x to X is given by:

$$X = R\,sin\frac{x}{R} \tag{4}$$

In order to use the undistortion function Eqn 4, we needed to know its parameter R. To that end, the coordinates of the circled points shown in Figures 3 and 4 were digitized and fitted to Eqn 4. X was digitized using pixel coordinates, while the units of length used for x was such that one unit separated each circled point. As a result of these two different length scales, the two R's in Eqn 4 have different numerical values, and were treated as two different parameters in the fit.

In this model, the image is laid out undistorted on the focus surface. Undistortion consists of obtaining this focus surface image from the CCD image by mapping coordinates from the former to the latter. We start with an empty array representing the focus surface. For each point in that array, we simply employ Eqn 4 to find the location in the distorted image that we should copy the grey level from. When the entire array has been filled, the undistortion is complete.

L. Averaging

The final preparation before a Fourier transform is to average each frame vertically. The height of a rectangle averaged was typically 2 or 3 pixels. This results in a one-dimensional array of grey levels along the length of the tube.

M. Fourier Transforms

At this point, we have an array of floating point numbers. Each row represents the surface brightness of the tube at a different time. 1D and 2D Fast Fourier Transforms were used. The 1D Fourier transform was applied separately to each row (i.e., that is, in the space direction only). This enabled us to study the time evolution of the Fourier modes in a run. The 2D Fourier transform was used only for Mixture B data, and was applied to the entire array. This enabled us to obtain separate Fourier modes for waves going in opposite directions.

Calibration of the grey level with respect to the local volume concentration of black sand indicates that, except for low black volume concentrations ($< 20\%$), the grey level is, to a good approximation, linearly related to the local sand concentration. As a result, before there is a significant presence of areas containing low black concentrations, the Fourier transform of the grey level data is directly proportional to that of the local sand concentration, except for the DC (zero frequency) bin, which is offset by an unknown constant that depends on the overall brightness of the image.

The resulting Fourier spectra were converted into Mathematica-readable files for visualization. Details of the specific analysis conducted is left to later sections.

II. OBSERVATIONS AND RESULTS

When the pyrex tube is rotated, interesting dynamical behaviour may be observed in the concentration profile of the sand and salt mixture. Here, in order of their temporal occurrence, we discuss the various granular dynamics observed: radial segregation, end segregation, travelling waves, and axial segregation. The latter two were studied in detail.

A. Radial segregation

When a non-monodisperse mixture of granular matter is rotated in a tube, the first thing that happens is radial segregation, a process in which smaller particles migrate radially inwards and form a core running along the length of the tube. It is easy to understand why this happens. MRI studies [16] show that the cross sectional flow of the tube may be divided into two regions, as shown schematically in Figure 6. Particles rotate collectively as a solid body in region A, but when they reach the top, they undergo shear flow down an incline (region B). During the flow, gaps may open up between particles, and since smaller particles have a higher probability of falling through those gaps, they naturally migrate towards the centre of rotation in the bulk of the grains.

For our system, radial segregation occurs rapidly, and has a time scale on the order of 10 rotations. So visually, the first thing that happens in our tube is that the overall mixture rapidly becomes lighter in colour as radial segregation takes black sand to the core. We did not study this effect in detail.

B. End segregation

End segregation is the formation of a band right by an end cap. This has been widely observed [12,18,13], but is still not understood. Like most previous reports, these end bands were composed of the smaller particles (the black sand) that formed right beside our teflon-covered end plugs. If, however, in a presegregated run, a white salt band started off against an end cap, then the band stayed white. The end bands form before other bands, and do not change for the duration of our runs, which were typically $\sim$1 hour.

Chicharro *et al.* [6] reported end bands that were stable even after two weeks of rotation, by which time the mixture had evolved to a fully segregated state with each species occupying one half of the tube. Their end bands, however, were composed of the larger particles instead of the smaller ones. The factors that determine which particles form the end bands are

unknown.

C. Description of travelling wave dynamics

The segregation phenomenon that has often been observed in the past [1,11,12,18] is easily seen in many different mixtures. In this laboratory, for instance, it has been seen in a binary mixture of different-sized glass beads and a mixture of green beans and rice.

What has never been seen are the travelling waves that precede the segregation in some mixtures. These travelling waves do not appear in Mixture A, but occur in Mixture B. The following discusses the observations and measurements made on these travelling waves.

D. Premixed initial conditions

Mixture B was used to study these travelling waves. For this mixture, the mixture ratio ϕ was varied over the range 0.33 - 0.79, while ω was held constant at $4.841 \pm 0.007 s^{-1}$. Figure 7 is a spacetime plot showing the travelling waves arising spontaneously from a uniformly mixed initial condition. As pointed out before, it is impossible to start with a perfectly uniform initial condition, so it is possible that an instability organizes initial concentration fluctuations into travelling structures that seem to have a preferred wavelength of about 45 $\pm$ 5 mm. These travelling structures move at fairly constant velocities and appear to pass through each other with little or no interaction, until segregation, which has been occurring in parallel, grows strong enough to interfere with and destroy them. Segregation produces the stationary black bands in Figure 7. These black bands appear to be saturated at 100% sand. As can be seen in Figure 7, the vicinity of these *saturated bands* are devoid of travelling waves. Travelling waves are dissipated in the vicinity of a saturated band.

E. Presegregated initial conditions

To control the initial condition, we performed experiments where we started the mixture off presegregated in a square wave concentration profile along the tube. This profile was one part black for every two parts white, yielding $\phi = 0.67$. Figure 8 shows an example of one such run. We see very clear oscillations between node and antinode, indicating a standing wave. Figure 9 shows the time-evolution of the Fourier transform of the tube's surface brightness. Structure occurs at wavenumbers corresponding to the presegregated wavelength. Each node of the standing wave in real space shows up as a valley between hills in Figure 9 since the amplitude of the standing wave is zero at a node.

By multiplying a Gaussian filter on to a two-dimensional Fourier transform of the space-time plot (Figure 10), and then inverse Fourier transforming, it is possible to extract the waves going in only one direction. The Gaussian has to be centred on the peak of interest, and its width selected such that the entire peak is contained without including unwanted modes. The result is shown in Figure 11. This figure shows that the travelling waves can be very robust and long-lived.

F. Travelling wave velocity measurements

In order to study how this velocity varies with wavelength, numerous runs were performed using the same mixture at different initial wavelengths, and the velocities of the resulting waves were measured. To avoid the effects of interactions with saturated bands that develop later, we measured the wave speed at early times only. This we did by measuring the time taken between the first and second nodes, which corresponds to half the period of the wave. The velocity was then obtained by dividing the wavelength by the period.

The time between the start of the rotation and the first node was not used as it is not clear what part of a period it corresponds to. In particular, it is likely to contain transients related to the relaxation of the presegregated square wave pattern into the travelling waves'

profile.

The resulting wave speeds as a function of presegregated wavelength are shown in Figure 12. Two other velocities obtained from a premixed run are included. These latter velocities were obtained from the angle of propagation of pairs of waves in the spacetime plot Figure 7.

An interesting feature of the waves as seen from the graph is that they stop travelling above a certain presegregated threshold wavelength. Figure 13 shows one such run, in which the presegregated bands are frozen right from the start. The following is a possible explanation. When the rotation is started, there is a brief relaxation phase in which the dark bands shrink as the sand near the interfaces spread away and sink towards the core. This is visible in Figure 13. It seems that travelling waves occur only when this shrinking completely submerges the black bands. For wavelengths at which no travelling waves occur, it was found that the centre parts of the black bands remained saturated with sand. Such pure bands are effectively impenetrable barriers to the movement of salt, and thus they cannot travel. Their appearance, immobility and stability indicates that they are the same saturated black bands that grow naturally in other runs.

Figure 14 shows the dispersion relation obtained from the velocity measurements.

The transition wavelength from travelling waves to frozen bands is difficult to pin down experimentally as, in its vicinity, we find a mixture of frozen bands and bands that begin to travel but merge when they meet (Figure 15). Some of these mergings seem more akin to absorption by saturated bands.

The amplitude of the travelling waves damps away with rotation, as shown in Figure 16a. Despite the change in amplitude, the velocity does not change (Figure 16b). This proves that the waves can be treated as linear waves. That these are linear waves is also supported by the fact that the waves travelling in opposite directions pass through each other, i.e., they superpose. The merging behaviour we see in Figure 15 indicates a loss of linearity near the transition from frozen bands to travelling waves.

Runs were also performed in which the initial wavelength was kept fixed while the mixture

ratio was varied. Figure 17 shows the velocity measurements from such runs. It can be seen that waves only travel for high mixture ratios, i.e., for high concentrations of salt.

G. Other structures

Some other interesting dynamical behaviour observed include pulses (Figure 18) and a 'fountain' (Figure 19), which sends out travelling waves in both directions. The pulse was prepared in the initial condition, but the fountain arose of its own accord; it is not known how to reproducibly make one.

Each pulse resembles a localized patch of travelling wave. When the rotation was started, each of the prepared white bands spontaneously pulled in black sand on their outer boundaries, then proceeded to travel away from each other. These two pulses also appear to be accompanied by fainter, co-travelling pulses on their sides.

The fountain appears to constantly send out travelling waves that disappear as they near the saturated bands on either side. If the saturated bands indeed absorb travelling waves, then it is possible that, eventually, the fountain would become depleted and cease. However, that did not happen during the 40 minutes that we observed the fountain.

H. Description of segregation dynamics

Unlike Mixture B, Mixture A does not produce any obvious travelling waves when run from a premixed initial state. Instead, it only exhibits axial segregation. A sample run is shown in Figure 20.

Mixture A was rotated at angular frequencies ω between 1.57 and 8.38 s^{-1} for 600 seconds, with 3 seconds elapsing between frame captures. No presegregated runs were conducted for Mixture A due to time constraints. As described above, radial segregation occurs rapidly, followed by end segregation. The first faint axial segregation bands can be visually observed after just a few tens of rotations. Except for high and low rotation rates, these bands intensify until the black bands saturate at 100% concentration. Three cases were

observed in which the black bands failed to saturate even when run for 1200 seconds: two occurred at high rotation rates ($\omega = 7.57s^{-1}$ and $8.38s^{-1}$) and one at a low rotation rate $\omega = 1.57s^{-1}$. These cases are discussed in later.

It is not known if there are white bands that achieve 100% concentration as a white band that appears to be 100% salt on the surface could still contain a black core that is not visible from the surface. On the other hand, from what is known of radial segregation, a band that appears on the surface to be saturated with the smaller particle species should consist only of that species all the way through. Nevertheless, we stress that, because we were restricted to surface observations, we were unable to confirm that the saturated black bands that we observe truly have only negligible amounts of salt in them.

I. Saturation

After rotating for some time, some black bands darken dramatically to the point where they appear to be composed of almost pure black sand. Bands do not all saturate at the same time; indeed, it has been observed that, if an area has a high local concentration at the start of a run, saturation commences earlier there.

For relatively high rotation rates ($\omega = 7.57s^{-1}$ and $8.38s^{-1}$), saturation was not observed at the end of 600 seconds. Further observations for another 600 seconds still did not yield saturated black bands. Later, we describe our reasons for believing that these runs may already have saturated even though the bands remained faint.

For the low rotation rate of $\omega = 1.57s^{-1}$, no saturation was observed at the end of 1200 seconds, but it is possible that they need more time to develop due to the slowness of the rotation. This possibility was not explored due to time constraints.

Saturated black bands are extremely stable over several thousand rotations. They were not observed to split. Only a few merging events have been observed between saturated bands, and they occur very slowly. Long runs were not pursued due to time limitations. Work done elsewhere indicates that the long time evolution of these bands favours merging,

and may result in complete segregation after a long time: after two weeks of rotation, Chicharro *et al.*'s system [6] reached a fully segregated configuration in which each species occupied one half of the tube.

Saturated black bands can sometimes be seen to absorb unsaturated ones (Figure 21). As travelling waves always disappear in the vicinity of saturated bands, it seems likely that they are absorbed by the latter as well. We have not directly observed this, and it will be difficult to do so by surface observation. Figure 15 does, however, provide evidence that this happens. In that picture, some dark bands near the centre split, as is usual for travelling waves, but they get absorbed into their neighbours. Note, however, that the bands that absorb the split bands were themselves shifted towards the split bands, almost as if they were ready to travel. As this shift does not occur in the case of saturated bands that dissipate travelling waves, Figure 15 may involve other mechanisms, and constitutes only partial evidence supporting the hypothesis that travelling waves are absorbed by saturated bands.

J. Band-dynamics

Before saturation, bands exhibit some interesting dynamics. Bands can disappear and appear, and they can merge and split. Examples of disappearance, merging and splitting are shown in Figure 20. It can also be seen from Figure 20 that, unlike Mixture B, this mixture's unsaturated bands are qualitatively different from the travelling waves: they are less mobile and, when they meet, they generally merge to form a darker band rather than pass through each other. In this respect, they resemble the behaviour of Mixture B at presegregated wavelengths near the transition from travelling waves to frozen bands.

A typical run (Figure 22) shows multiple Fourier peaks that emerge during the period of band dynamics. Spectra with multiple modes with no one mode dominant are common.

K. Segregation as increase in power in Fourier modes

Figure 22 shows that segregation leads to growth in various Fourier modes. In order to characterize this growth, we consider the change in the size of Fourier peaks with time. Figure 23 is typical of modes in our Fourier spectra. Its growth can be characterized as being approximately exponential initially, but experiencing saturation.

It was discovered that the growth of the total power in the Fourier spectrum, less the first 5 bins to eliminate the DC component, is also well-described as being exponential initially (Figure 24). It ceases to grow exponentially at a certain point in time. And when this point in time was examined in the original spacetime image, it was found to correspond to the onset of saturation.

Although individual bins *and* the total power grow approximately exponentially with time, the total power is *not* dominated by any one bin, as shown for two sample runs in Figure 25.

There were two exceptions at high angular velocities ($\omega = 7.57s^{-1}$ and $8.38s^{-1}$) where saturation did not occur within the duration of the experiment, but a saturation-like loss of exponential growth was still observed. The bands we observed stayed faint. We hypothesize that a mechanism like the randomizing diffusive effects of high rotation rates limits the growth of these bands at those higher speeds.

We will call the exponential growth rate of the total Fourier spectrum, less the DC component, the *structural growth rate*. Structural growth rates were plotted versus angular frequency, and the results are shown in Figure 26. There is a clear maximum rate of structure creation at $\omega \simeq 4s^{-1}$. We note, moreover, that the structural growth rate depends on the angular velocity.

L. Selected modes

The saturated bands usually occur at fairly regular spacings. This observation can be made visually, and suggests a characteristic wavelength, or a range of characteristic wavelengths, for the bands in the tube. To examine the existence of these wavelengths, the Fourier spectra of the runs for various ω's were examined at the onset of saturation as determined by the loss of exponentiality discussed in the last section. Examining the Fourier spectra before saturation is not useful as the relative size of Fourier modes is still changing due to band dynamics.

As the resulting spectra are noisy, they were averaged together. Each individual spectrum was first normalized by dividing by the total power outside DC. Figure 27 shows the resulting spectrum with a peak at 52 mm. This is evidence for a selected wavelength, with a possible secondary peak at 68 mm. A second plot was also made of the peak wavelengths. As there were sometimes multiple peaks of almost equal size, centre-of-mass wavelengths were also obtained to more accurately take the spread into account. The centre-of-mass was obtained over a range of wavenumbers from just above DC to twice the peak wavenumber. The result is shown in Figure 28. It shows that, to a first approximation, the selected wavelengths are independent of rotation rate, at least in the range of rotation rates examined.

M. Rocking Segregation

In this section, we briefly describe a new type of segregation that was observed, but which could not be investigated for lack of time. When the tube was rocked back and forth at a frequency of $\sim$2 Hz, and with enough amplitude that the material inside spent a large fraction of each cycle in flight, surprisingly regular bands of very short wavelength (18 mm) appeared. To our knowledge, this is the first observation of such an effect. The appearance of the bands is surprising because the vigorous motion of the grains would be expected to have a powerful randomizing effect rather than an organizing one.

N. Latebreaking results

Recent work done on the system using Mixture B by Michael Baker, an undergraduate summer student, has found that the travelling waves are robust for filling factors 25% and 50% higher than the ones used for this thesis. He has also measured the travelling waves' speeds as a function of ω and found that the bands in a presegregated run freeze above about $\omega = 6.3$ Hz, but travel for slower rotation rates. Finally, he has also found that, in the travelling regime, the speeds at which the waves travel do not have a strong dependence on ω.

III. DISCUSSION

A. Impediments to reproducing travelling waves

The salt used starts off with its normal white colour. However, with use, it slowly acquires a greyish appearance. Casual observation might lead one to think that the black sand was dirtying the salt, but scrutiny under a microscope has revealed that the change in appearance is due to repeated use in experiments that leads to surface polishing and increased transparency. This surface smoothening may be required for the occurrence of traveling waves, as it has been observed anecdotally that salt fresh out of the box does not travel well, but works better after a few runs. The existence of this maturing period could potentially be an impediment to future attempts to reproduce this work.

Preliminary results from Michael Baker, our undergraduate summer student, indicates that the travelling waves are obtained for sand between 180 and 250 μm works. However, other sizes do not work. Thus, the existence of travelling waves shows some sensitivity to the sizes of the particles used.

It is also not known if travelling waves occurs in mixtures other than sand and salt. To the author's knowledge, no previous work has been done using sand and salt. Given the

robustness of the other phenomena in this system, however, it is unlikely that our travelling waves are specific to sand and salt only.

In the author's view, it is possible that some previous workers might have had the opportunity to see these waves, but did not because travelling waves are faint and are actually quite easy to discount as perturbations if one simply uses visual observation. In this respect, the sensitivity of the CCD camera and the construction of a spacetime picture were invaluable in the detection of faint bands because they show up indisputably as a stripe running across a spacetime plot.

We have seen that a high mixture ratio is necessary to achieve travelling waves. Thus, another reason past workers might not have seen travelling waves is because they typically worked at a mixture ratio of 0.5.

B. Discussion on experimental findings

Like other workers, we have observed axial segregation in a regime of streaming flow. Like others, we have also observed merging, splitting, band appearance and band disappearance. We have also observed radial and end segregation.

Fauve *et al.* [26] have observed an oscillatory instability of the streaming surface and undulation modes of the lower contact line in experiments with single-species sand. As far as can be determined visually, these motions do not occur in our system. Furthermore, these motions occurred on a timescale comparable to one rotation period, which is much shorter than the period of a travelling wave, which is $\sim$100 rotations. Therefore, it is likely that Fauve *et al.*'s effect involves a mechanism different from that of the travelling waves'.

Using glass beads, Zik *et al.* observe that the bands evolve gradually into a 'steady state'. This is likely to correspond to a tube consisting of saturated bands. Previous workers did not distinguish between saturated bands and unsaturated ones. Saturated bands are very stable. Whereas unsaturated bands undergo merging amongst themselves, saturated bands can *absorb* unsaturated ones, and may absorb travelling waves as well. Future work must

distinguish between them due to their widely different behaviours.

On a longer timescale, the saturated bands are reported to display a tendency to merge: Chicharro *et al.* [6] found that, for a mixture of different-sized Ottawa sand, the mixture segregated fully into two bands after about two weeks. The time of our observations was typically on ∼1 hour, and was too short to verify their findings.

Hill *et al.* [18] report that, for some mixtures, the axial segregation effect disappears at low rotation rates, while for some others, axial segregation was always present. Hill *et al.* and Das Gupta *et al.* [13] link the onset of axial segregation to the appearance of a nonzero dynamic angle of repose difference between the two particle species. In our system, axial segregation was always present.

Previous workers [1,13,15], by counting bands, report that the number of bands decreases with increasing rotation rate. This means that the wavelength increases with increasing rotation rate, whereas we find that the wavelength is independent of the rotation rate. We suggest that, with CCD camera imaging and image division, we are able to capture faint bands that were missed by previous authors, particularly the ones that fail to saturate at high rotation rates (as discussed in Observations). MRI work [19] has shown that subsurface bands exist. While hard to observe, it is believed that, in this work, we are often able to detect these subsurface bands because of the good statistics allowed by our long data capture times. We conclude that, by taking into account faint bands that had previously been missed, we find that the selected wavelength is independent of rotation rate.

Finally, we note that Mixture B goes from travelling wave behaviour to merging behaviour when the wavelength or mixture ratio is increased. We speculate that Mixture A's unsaturated bands, which merge but do not travel, reside in its merging regime, and that travelling waves may exist for lower mixture ratios and/or smaller wavelengths.

C. Existing models

Apart from Zik *et al.* [17], not much theoretical modeling has been attempted on the rotating tube system. The simple models of axial segregation most commonly constructed derive from the continuity equation [14]:

$$\partial_t c = -\partial_x J, \tag{5}$$

where $J(c, x, t)$ is the axial concentration current. It is usually assumed that J has the form

$$J = (\beta - D)\partial_x c, \tag{6}$$

where $D > 0$ is the usual Fick diffusion coefficient and $\beta(c, x)$ describes the tendency of the mixture to segregate. If $\beta(c, x)$ is a constant and $\beta > D$, Eqn. 5 reduces to a diffusion equation with a negative diffusion coefficient, so that initial concentration fluctuations grow, leading to areas of high concentration that might correspond to the bands observed experimentally. Various assumptions for $\beta(c, x)$ define a class of nonlinear segregation models. In models where surface effects are proposed as the segregating mechanism, $\beta(c, x)$ is presumed to be related to the difference in the dynamic angles of repose of the two components. Das Gupta *et al.* [13] and Hill *et al.* [18] have seen evidence of the cessation of segregation when the rotation rate was low enough that the dynamic angle of repose difference between the two species disappeared.

The most complete theory of axial segregation as a consequence of surface slope effects is that of Zik *et al.* [17] for which $\beta(c) \propto c(1 - c)$. Although this model has its successes, such as obtaining an S-shaped cross-sectional profile of the flowing sand that is qualitatively similar to experimental observation, there is currently no agreement on whether the axial segregation is a surface effect, or if the core is responsible. As a result, tests of the validity of the assumptions used in this model must await further experimental study, particularly MRI ones.

These models, plus a simple cellular automaton one [14], cover all that have been proposed so far in the literature [14,18,17], and they are consistent with what has hitherto been

known about axial segregation before this work. However, as these theories do not predict selected wavelengths, nor do they support travelling waves for real concentrations, they are invalidated by our key findings.

The fact that there are selected wavelengths, pulses and sources in the system shows that it can be viewed as a pattern formation system. The theory of this system, and of most granular systems for that matter, is very undeveloped. We suggest adopting a pattern formation view so that we can use its conceptual framework to guide future efforts. In particular, it might provide the starting point for a phenomenological model.

D. The rotating tube as a pattern forming system

In the last section, we suggested that this system can be viewed as a pattern forming system. In this section, we consider such a viewpoint, and discuss the implications.

In pattern forming systems, a spatially extended system that is translationally invariant undergoes a bifurcation to a patterned state when a control parameter increases from negative to 0. The control parameter is a number that is calculated from physical variables, and the mapping from the physical variables to the control parameter is such that the latter is 0 at onset.

The control parameter also helps to control how fast a pattern grows. The fact that the structural growth rate depends on the rate of rotation ω shows that the control parameter depends on ω. The natural question to ask, then, is if there is a critical frequency, just as there is a critical temperature difference in Rayleigh-Benard convection. However, a critical frequency was not located: segregation was observed at all rotation rates investigated. Nevertheless, working with glass beads, Das Gupta *et al.* [13] and Hill *et al.* [18] have found a cutoff frequency below which there is no segregation. This was true for some mixtures, but not others. For the latter group of systems, the control parameter may become 0 at a rotation rate outside the physically attainable range. The same may apply to ours as well. More studies are needed to discover the variables that this control parameter depends on,

and the situations under which onset lies within an attainable range of angular frequencies.

Being able to study the system at onset is important because it is known that, near onset, some pattern formation systems may be described theoretically by simple equations of universal form, such as the Ginzburg-Landau equation [2].

Now that we have evidence that there is a selected wavenumber, it would also be of interest to find out what the variables that control it are. Das Gupta *et al.* [13] have found that increasing the volume fraction of the smaller particles seems to increase the number of bands, that is, it seems to reduce the wavelength. Future work should investigate this dependence of the wavelength on the mixture ratio.

Several of the structures observed in our experiment correspond to ones described in pattern formation literature, such as [28], *sources* that send out *travelling waves*, which travel and disappear into *sinks*. A fountain corresponds to a source, while a saturated band may correspond to a sink. *Pulses* have also been observed in other systems [29,28]. Further studies are needed to understand the properties of these structures, and how they can be created.

E. Constraints on a theory

In this section, we discuss constraints that our observations put on future theories that attempt to model this system. First, we consider a phenomenological theory, which, like those proposed before, uses a single scalar variable to represent the concentration at each point in the tube, and uses only one spatial dimension x (in the axial direction). This is very simplistic, and neglects the radial distribution of material. We note also that Zik *et al.*'s [17] model also does not take into the radial distribution of material, even though a two-dimensional model serves as the starting point.

We have stopped the tube at a node in a standing wave, and then restarted it. Apart from mild distortions that can be attributed to disturbances due to the jerk at the stop and the start, the standing wave continued on. This implies that the time rate of change of

the pattern is not important as an initial condition, and therefore, assuming that a partial differential equation governs the system, *it must be first order in time.* We will call this PDE the *target PDE* .

Symmetries of the system should also be taken into account. The system is invariant under translation and reflection in space. This implies that the target PDE cannot explicitly contain x, and that all spatial derivatives of the concentration must be of even order, or even power.

As is common in pattern formation studies, we can associate a phase angle with each point of the pattern. A travelling wave would then be:

$$c = Ae^{i(\omega t - kx)} \tag{7}$$

This is justifiable due to the periodic nature of the pattern observed. Thus, we can use the real part of a complex number to represent the concentration at each point. And since the pattern state must continue to satisfy the target PDE under translation in space, and translation in space can be implemented by shifting the phase at all points by the same amount, we conclude that the target PDE must also be invariant under phase shift in concentration.

Another constraint comes from the fact that, in the dispersion relation for the travelling waves, ω depends on k. We illustrate our point using the Ginzburg-Landau equation, which is commonly used in pattern formation studies for modes near some selected mode. The Ginzburg-Landau equation prescribes the growth of an amplitude $A(x,t)$ of the selected mode with wavenumber k_c and frequency ω_c. $A(x,t)$ is allowed a slow space and time dependence to represent a mode that is close to (k_c, ω_c), and it looks like:

$$A(x,t) = A_0 e^{\gamma t + i[(\omega - \omega_c)t - (k - k_c)x]} \tag{8}$$

The Ginzburg-Landau equation is:

$$\tau_0 A_t = \epsilon A + \xi_0^2 A_{xx} - g|A|^2 A \tag{9}$$

If one puts Eqn. 8 into Eqn. 9 and equates real and imaginary parts, one gets that:

$$\gamma = \frac{\epsilon - \xi_0^2(k-k_c)^2 - g|A|^2}{\tau_0} \tag{10}$$

$$\omega = \omega_c \tag{11}$$

One sees that ω would need ξ_0^2 to be complex in order to have a k-dependence. In general, at least one spatial derivative term in the target PDE must have a complex coefficient in order that the dispersion relation have a wavenumber dependence.

In fact, the complex version of the Ginzburg-Landau equation, which has complex nonlinear and second spatial derivative coefficients (corresponding to g and ξ_0^2 in Eqn. 9) has been shown to exhibit sources, pulses and sinks [28]. While the evidence is qualitative, it does hint that the complex Ginzburg-Landau equation or something else similar to it might apply to the system in a first macroscopic phenomenological theory.

F. The complex Ginzburg-Landau equation

In this section, we consider the possibility that the Complex-Ginzburg-Landau equation might illustrate the phenomenology of our system. We stress that the Ginzburg-Landau equation is generally only true near onset [2], and it is not known if it applies here.

Unlike the real Ginzburg-Landau equation, the complex version has complex nonlinear and spatial derivative coefficients:

$$A_t = \epsilon A + (1+ic_1)A_{xx} - (1-ic_3)|A|^2 A \tag{12}$$

where a time, space and amplitude rescaling has been applied to reduce the number of coefficients. It is easy to check that, as observed experimentally, exponential growth occurs for all modes, and that they saturate. We find, moreover, that a solution of the form Eqn. 8 leads to:

$$\gamma = \epsilon - (k-k_c)^2 - |A|^2 \tag{13}$$

$$\omega = \omega_c - c_1(k - k_c)^2 + c_3|A|^2 \tag{14}$$

which supports a bifurcation to a travelling wave state when k is tuned such that ω becomes positive. We also note from Eqn 13 that wavelength selection is supported, as different wavenumbers grow at different rates, with k_c growing fastest. This resembles experiment observations.

We also note that the invariance under spatial reflection of Eqn. 12 means that it can support bidirectional travelling waves.

As discovered experimentally, the wave speeds are independent of the amplitude. This means that these waves will closely satisfy a linearized version of the governing equations, and thus be able to form standing waves under superposition. Thus, working with the linearized form of Eqn 12, Eqn. 14 becomes:

$$\omega = \omega_c - c_1(k - k_c)^2 \tag{15}$$

which yields a prediction for the dispersion relation. This predicts a quadratic form for the dispersion relation with a turning point at $k = k_c$, which presumably is the frequency of the spontaneous waves in Figure 7. There is a hint of a turning point in the dispersion relation Figure 14 near the selected frequency, but unfortunately, insufficient data exists at this time to allow us to claim that. There is definite room for future work here.

G. Granular physics-based models

We now turn from phenomenological models to physical ones. If we consider the cross-section of the tube (Figure 6), we see that particle transport occurs in the flowing layer. Thus, a good model for the flowing layer should lead to an understanding of travelling waves as well as axial segregation.

A good starting point is to consider a two dimensional rotating drum. The drum is two dimensional in the sense that it is only 1 particle deep in the axial direction. Because of this spatial reduction, this system is easier to study and understand. However, the exact method

of approach is still in question. It is not known if a continuum approach, so successful in fluids, applies to granular matter. And unlike fluids, there are no agreed-upon starting point for fundamental equations.

Khakhar *et al.* [21] have recently devised a continuum model that is fairly successful at predicting the thickness of the flowing layer. This model has one adjustable parameter: the interparticle collision stress. So there is hope that the flowing layer in the extended 3D tube may be modelled using a continuum approach like this.

Other approaches might yield fruit as well. Experiments in the 2D drum by Clement *et al.* [22] hints that a stochastic view might work. By observing a single tracer particle, they show that the radial position of a particle can be viewed as being determined stochastically by a Markov process.

As Das Gupta *et al.* [13] have pointed out, axial segregation is always preceded by radial segregation, and the latter could well determine the properties of, or even be necessary for, the former. Likewise, travelling waves could depend on radial segregation as well. In particular, the smaller particles are expected to be less mobile axially. This is because they tend to stay near the core, and hence enter the flowing layer near its midpoint. There, particles only flow a short distance in the flowing layer before being frozen in the lower bed, as illustrated in Figure 29. Thus, two factors impede axial transport for small particles: the small particles spend more time locked in solid rotation than the large particles, and during the flowing phase, the small particles are less mobile in the axial direction than large particles because the tighter packing nearer the bed constrains motion.

The flowlines shown in Figure 29 are *tendencies* only: they do not retrace perfectly. They can be observed in streak photographs [21], or by eye when coarse particles are used. Clement *et al.* [22] have also shown that they tend to retrace.

IV. FUTURE WORK AND CONCLUSIONS

A. Future work

In this section, we point out the directions for future work on this system.

Immediate work may be done on obtaining more data points for the dispersion relation to see if there is indeed a turning point near the selected travelling mode.

An interesting question concerns the transport properties of the material in a travelling wave: if one follows the motion of a dark crest of sand, does the material composing it move coherently with it, or not? This question can be answered by presegregating the tube as usual except for a single band which contains sand of a colour that is easily distinguished from the regular sand and the salt.

Also, a narrower size distribution of the sand and salt should be obtained if possible, as it might make the experiment easier to compare to eventual theories, and possibly yield cleaner data.

From the pattern formation point of view, it is interesting to determine the other variables that form the control parameter controlling axial segregation. Variables that determine the selected wavelength and frequency are also important. Obvious variables are the ones that define the system geometry: the length of the tube, and its radius.

The difference between Mixture A and Mixture B needs to be clarified. Are they fundamentally different? Or do Mixture A's unsaturated bands exist in Mixture B's merging regime as we have speculated? Travelling waves should be sought in Mixture A at lower mixture ratios and shorter wavelengths.

Travelling waves are faint, likely because they are primarily subsurface. Therefore, a tool like MRI is ideal for studying it. An immediate question that may be addressed is if travelling waves are indeed absorbed by saturated bands. MRI-active samples that show travelling waves will need to be found, however.

We have barely scratched the surface of structures like pulses and sources and sinks.

Further work can be done characterizing their properties and their mutual interactions. Once again, MRI might prove to be the ideal tool for tracking them in their entirety. Moreover, various presegregation states can also be attempted. We have only tried periodic and pulse seedings. It is possible that various structures can be reliably generated by the appropriate seeding.

From a granular matter point of view, the role played by various material properties (such as the angle of repose, surface roughness, etc.) is interesting. The dynamic angles of repose of our two materials may be measured to see if indeed they are different at all rotation rates and so cause the mixture to always segregate.

B. Summary and Conclusion

For this thesis, we have studied the dynamics of a binary granular mixture in a rotating tube. Like previous workers, we have observed radial, end and axial segregation, as well as merging and splitting dynamics; in addition, we have observed travelling waves, which is new.

We have measured the dispersion relation of the travelling waves, and also the velocity dependence on the mixture ratio. We have found that waves stop travelling above a wavelength cutoff and below a mixture ratio cutoff. In between the travelling regime and the frozen regime, we find merging behaviour. We have also shown that the waves can be treated as being linear because the wave speed is independent of amplitude.

We have also observed travelling pulses and sources. Saturated black bands may behave like sinks.

We have examined the growth of the segregation bands. From Fourier analysis, we were able to determine that the system experiences wavelength selection that is independent of rotation rate, and that the growth in structure varies with rotation rate, and has a peak at about $\omega = 4$ Hz. We have shown that our method of quantifying structure is useful for determining the onset of saturation.

This granular system has shown itself to be the source of rich behaviour. Experimentally, more work needs to be done to better document and understand its many properties. Theoretically, our observation of travelling waves invalidates previous theories about the system, so there is a need for work to model the rich dynamics of the system.

Because of its wavelength selection and other pattern forming properties, we have suggested that the system may be viewed as a pattern forming system. Working in this framework will help focus the efforts of future researchers.

FIGURES

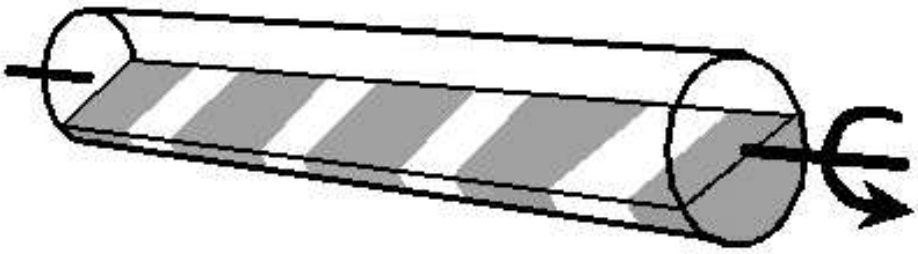

FIG. 1. Schematic diagram of tube containing sand which has segregated into alternating bands.

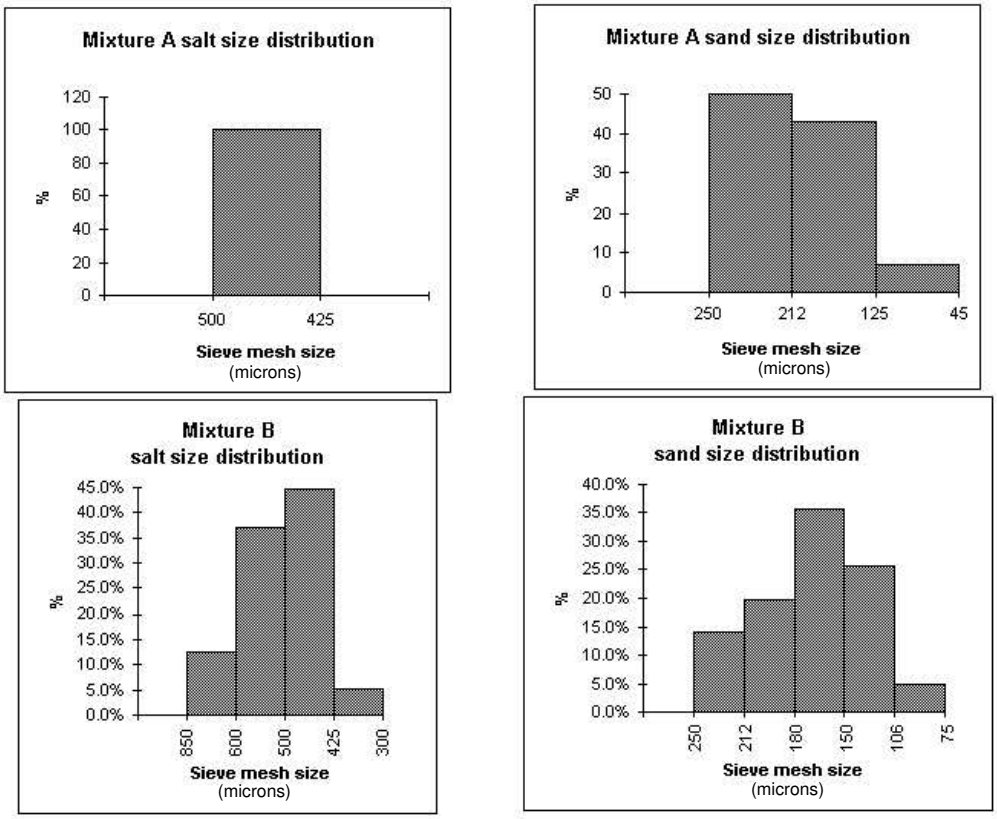

FIG. 2. Histograms of sand and salt sizes in mixtures A and B. Scale does not appear linear because sizes labelled correspond to sieve mesh sizes, which were not spaced linearly.

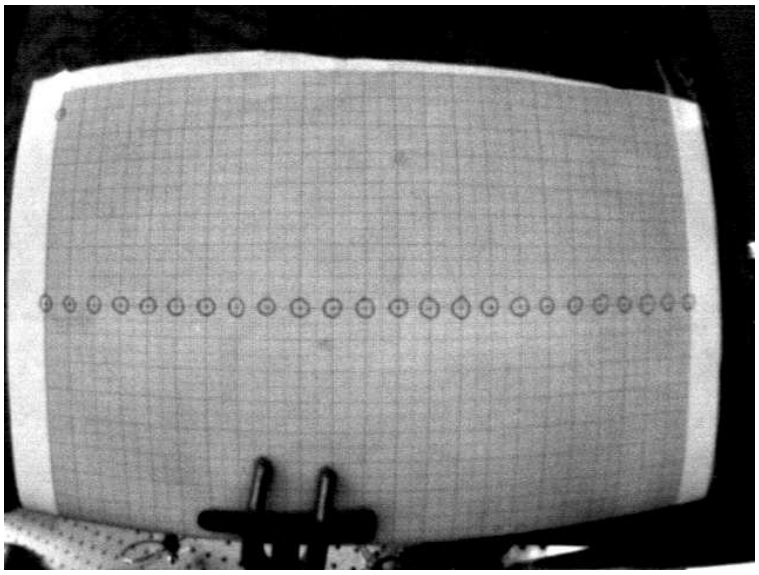

FIG. 3. A grid before correction.

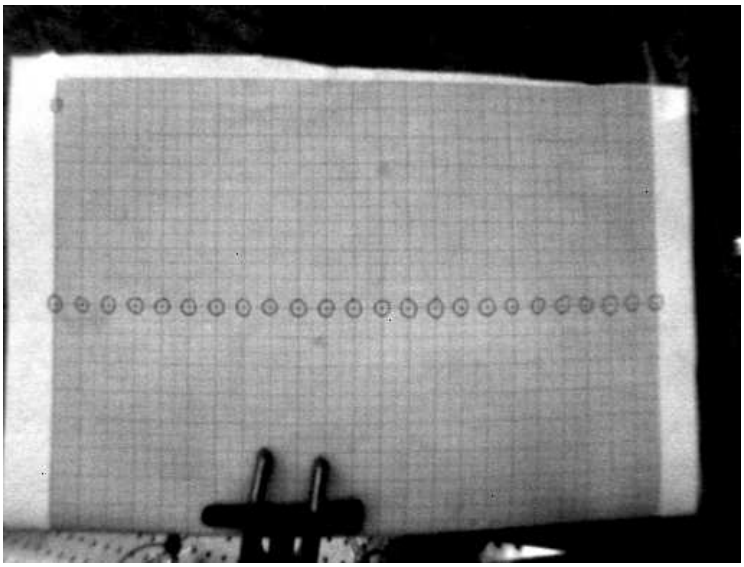

FIG. 4. The same grid after correction.

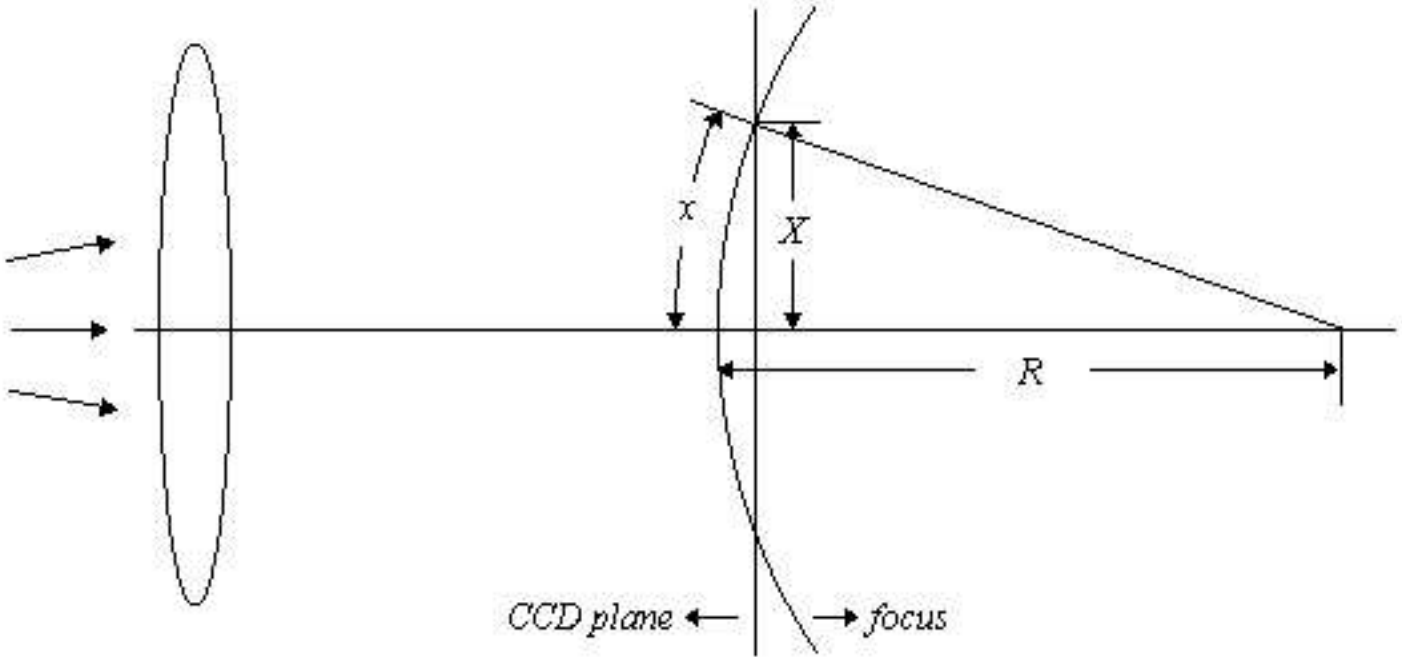

FIG. 5. Simple model for distortion in CCD camera

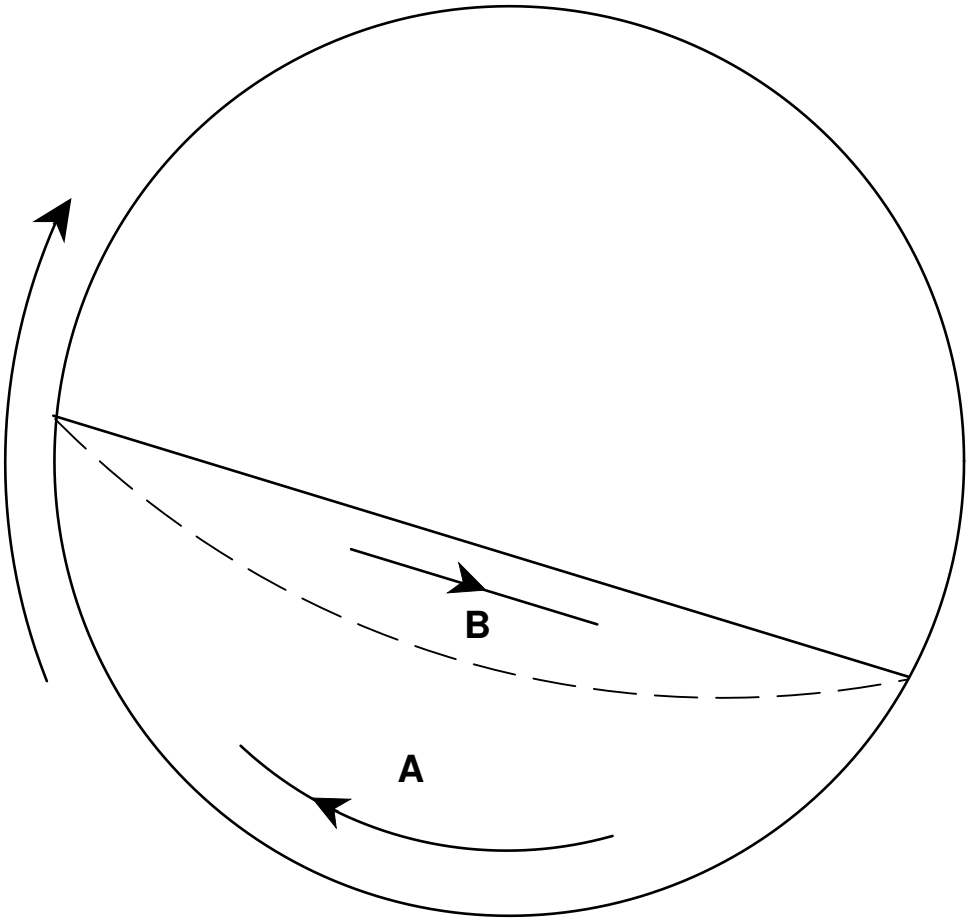

FIG. 6. Cross section of tube showing the region of solid-body rotation (A) and shear flow down an incline (B).

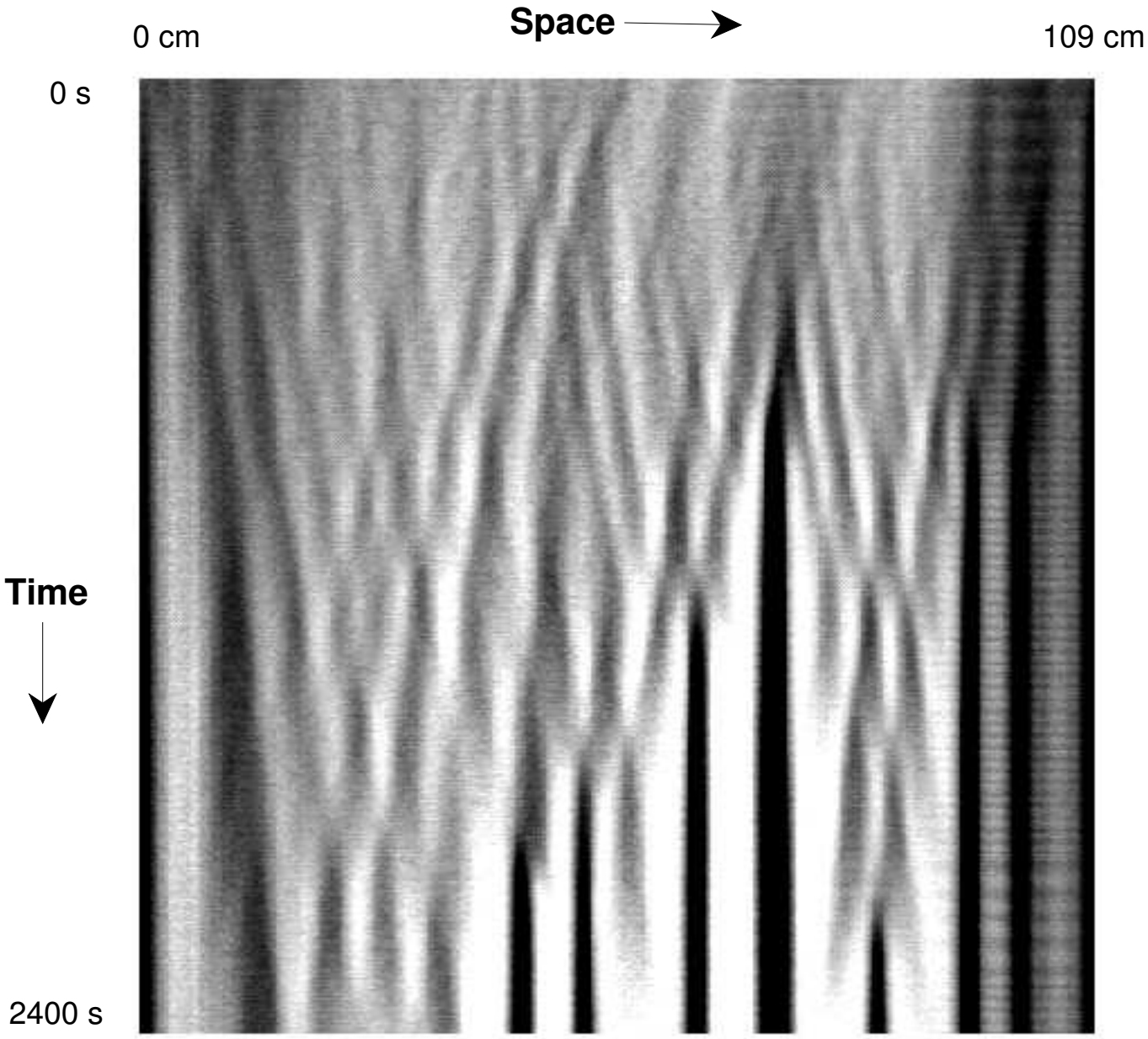

FIG. 7. Travelling waves arising spontaneously from a uniformly mixed initial condition. $\omega = 4.841 s^{-1}$ and $\phi = 0.67$.

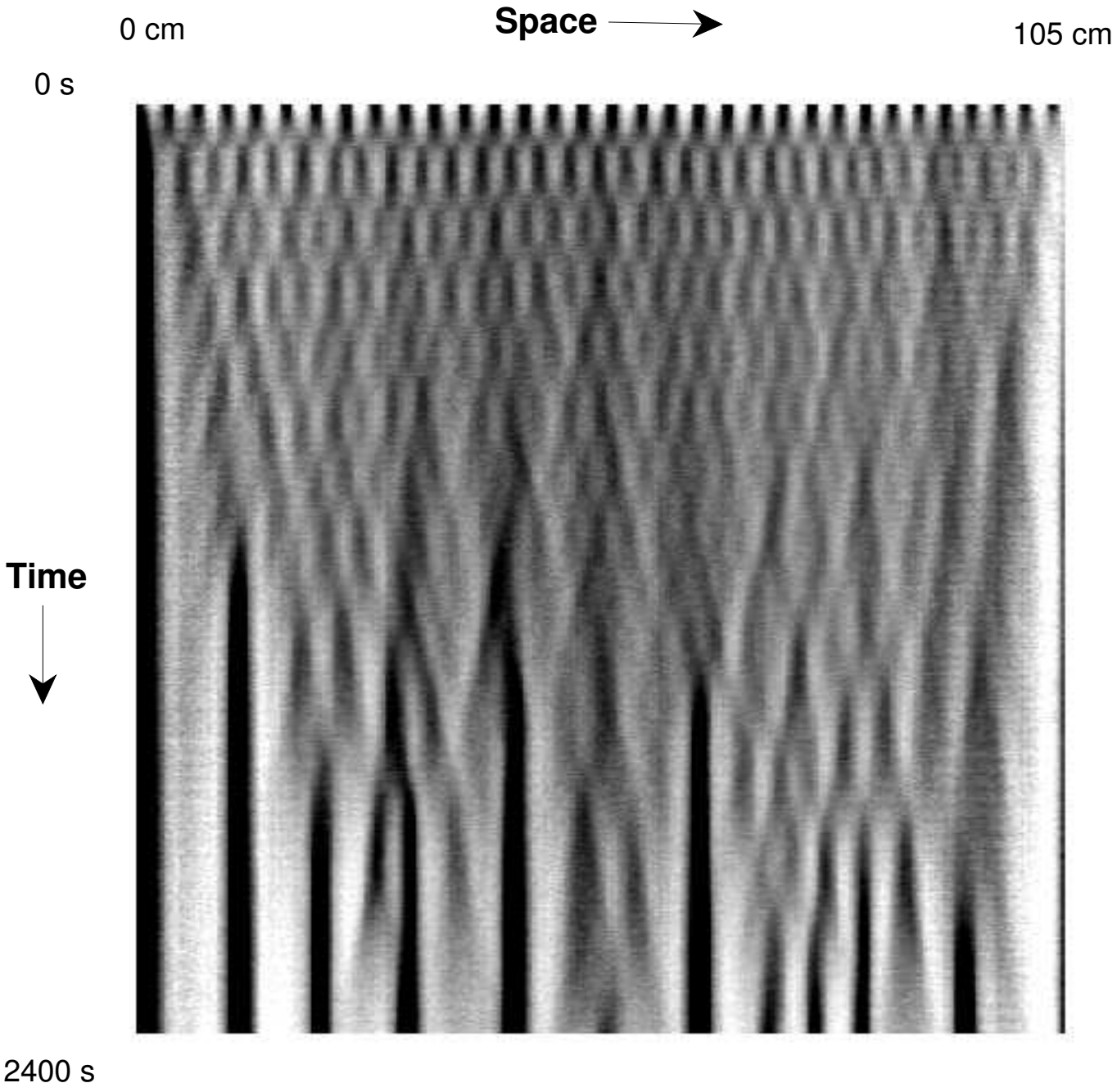

FIG. 8. Standing waves in a presegregated initial condition. $\omega = 4.841 s^{-1}$ and $\phi = 0.67$.

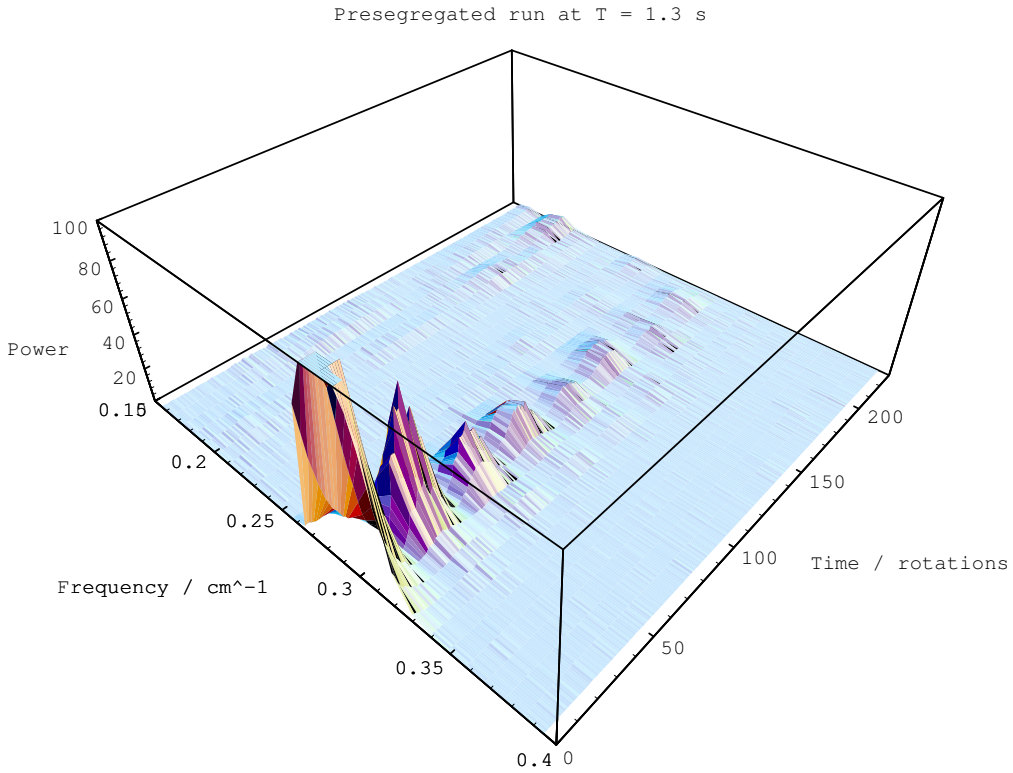

FIG. 9. Time evolution of the Fourier spectrum of the previous figure. Standing waves showing up clearly as hills when the space direction is Fourier transformed. $\omega = 4.841 s^{-1}$ and $\phi = 0.67$.

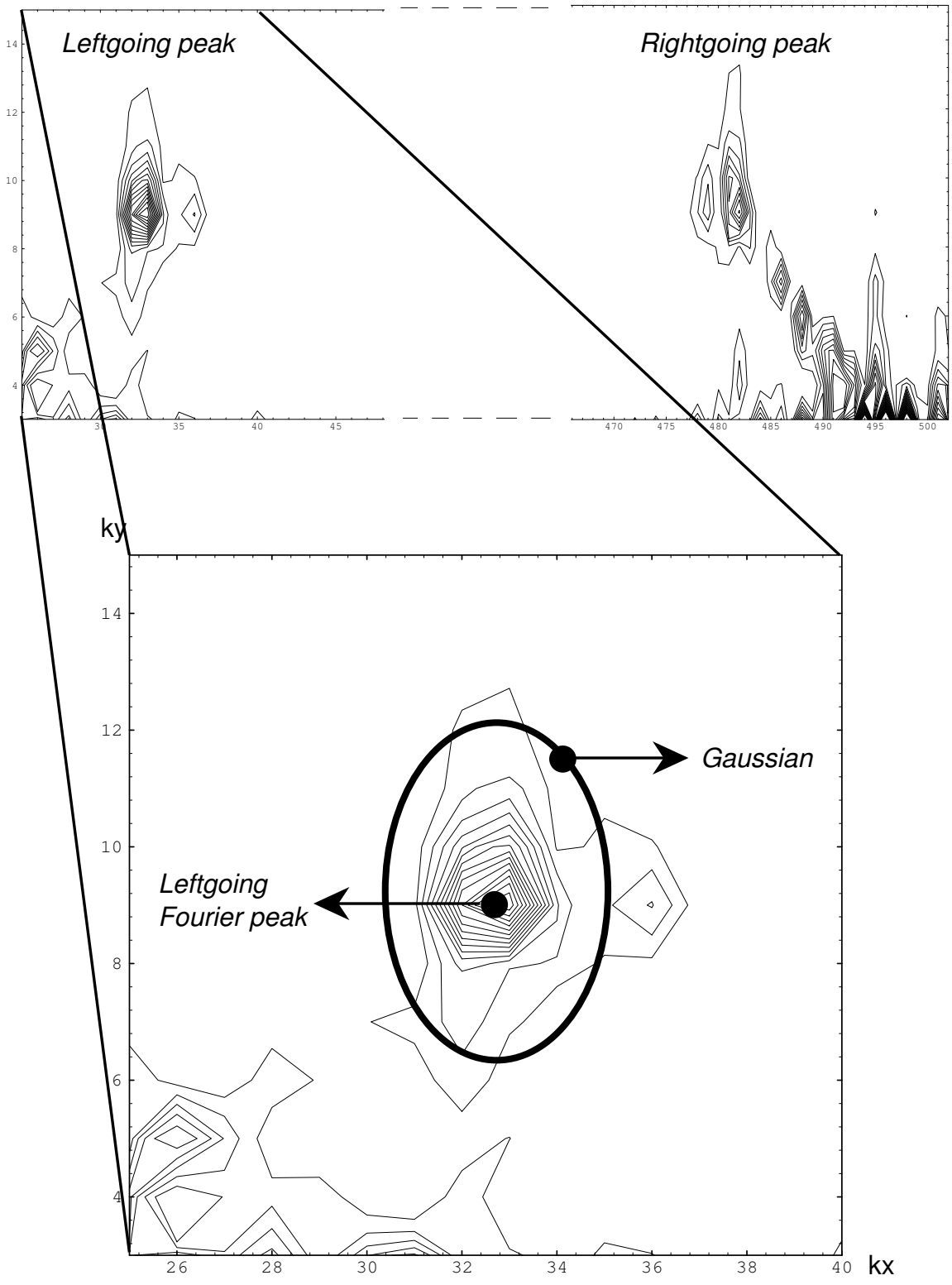

FIG. 10. Gaussian filter centred on the 2D Fourier mode corresponding to a travelling wave in one direction extracts just that mode.

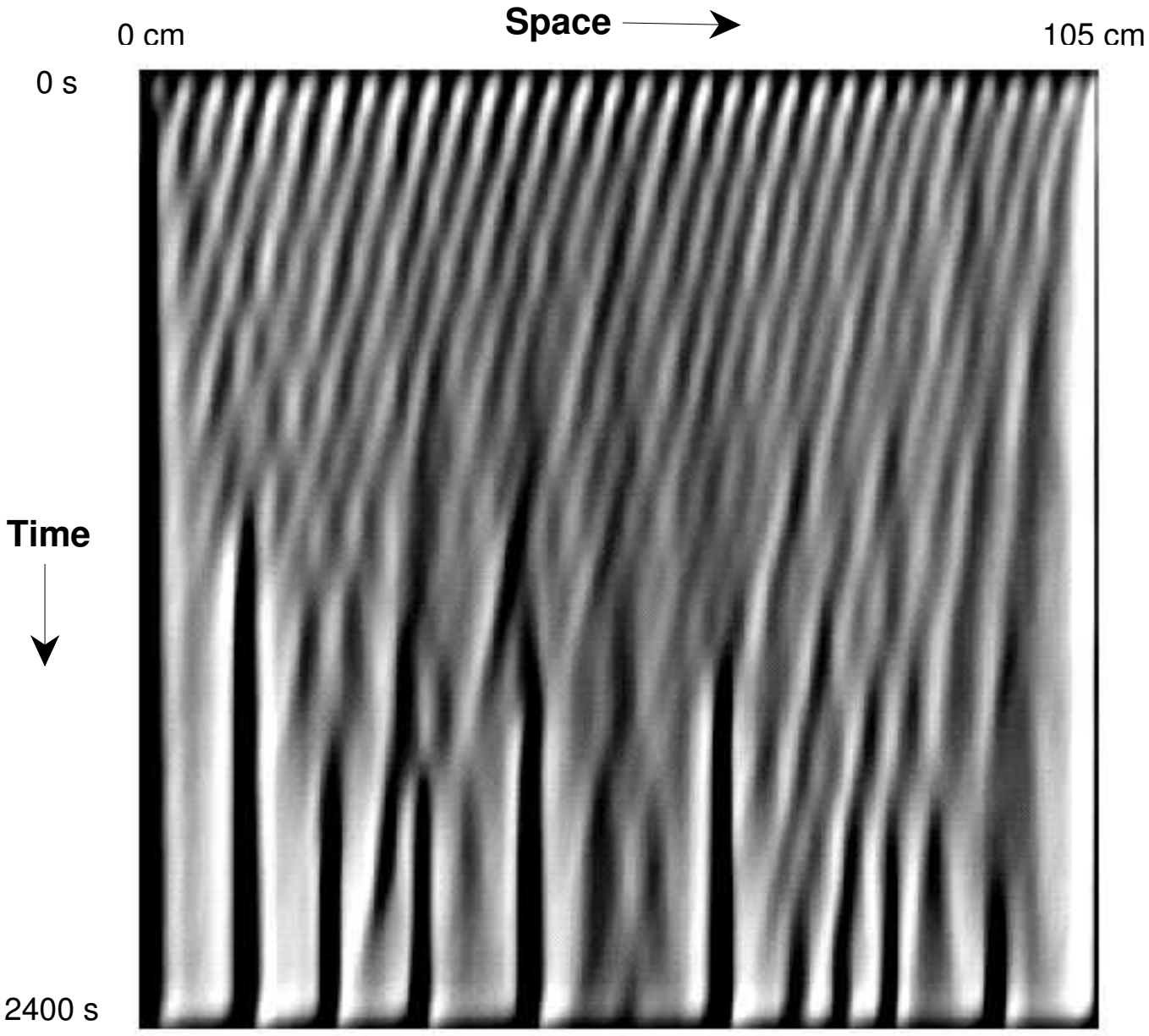

FIG. 11. Left-going waves extracted from a presegregated run using a gaussian filter.

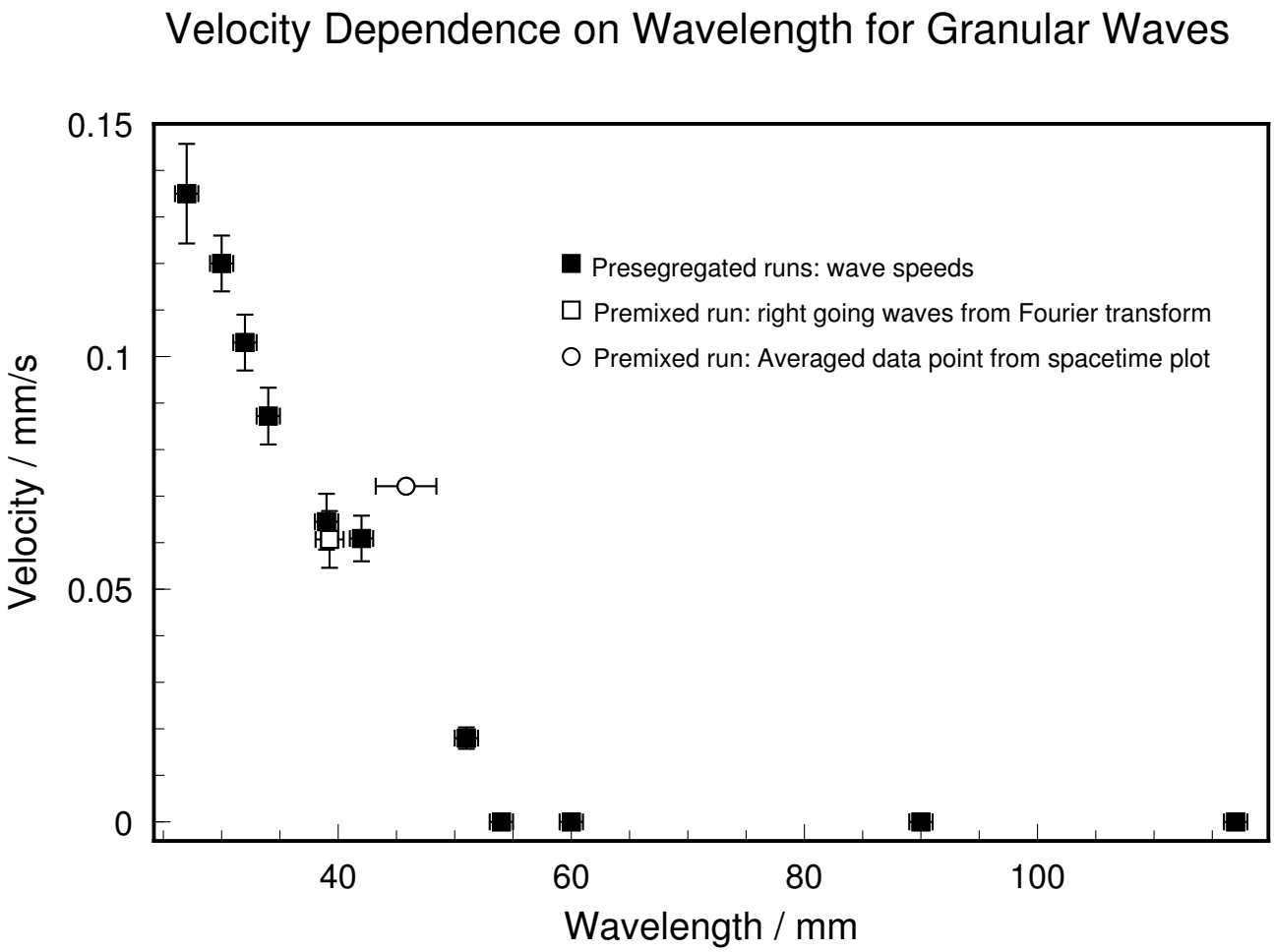

FIG. 12. Graph showing drop in velocity with increasing wavelength. $\omega = 4.841 s^{-1}$ and $\phi = 0.67$.

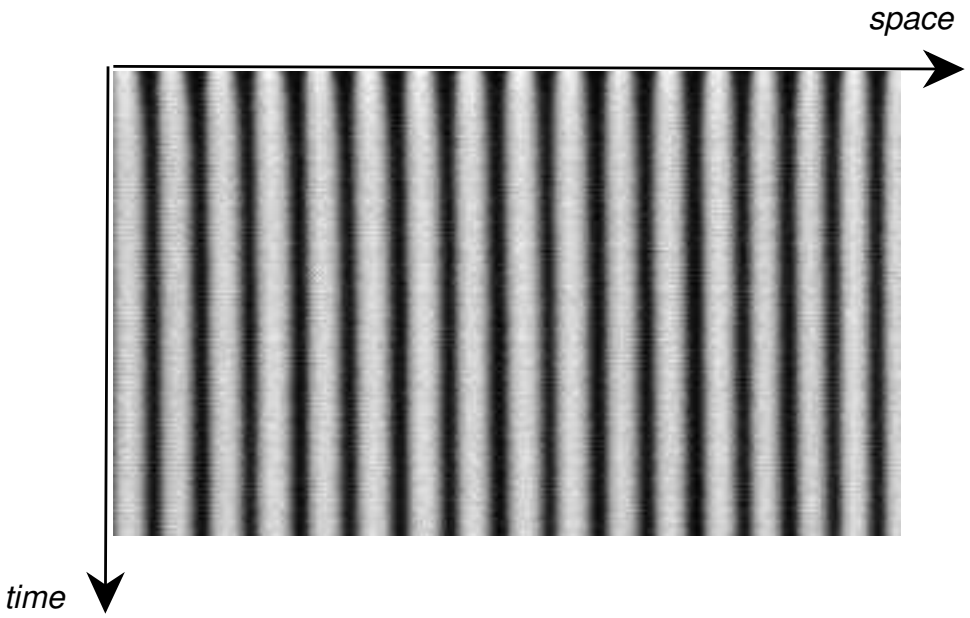

FIG. 13. A run in which the presegregated bands do not travel. $\omega = 4.841 s^{-1}$ and $\phi = 0.67$.

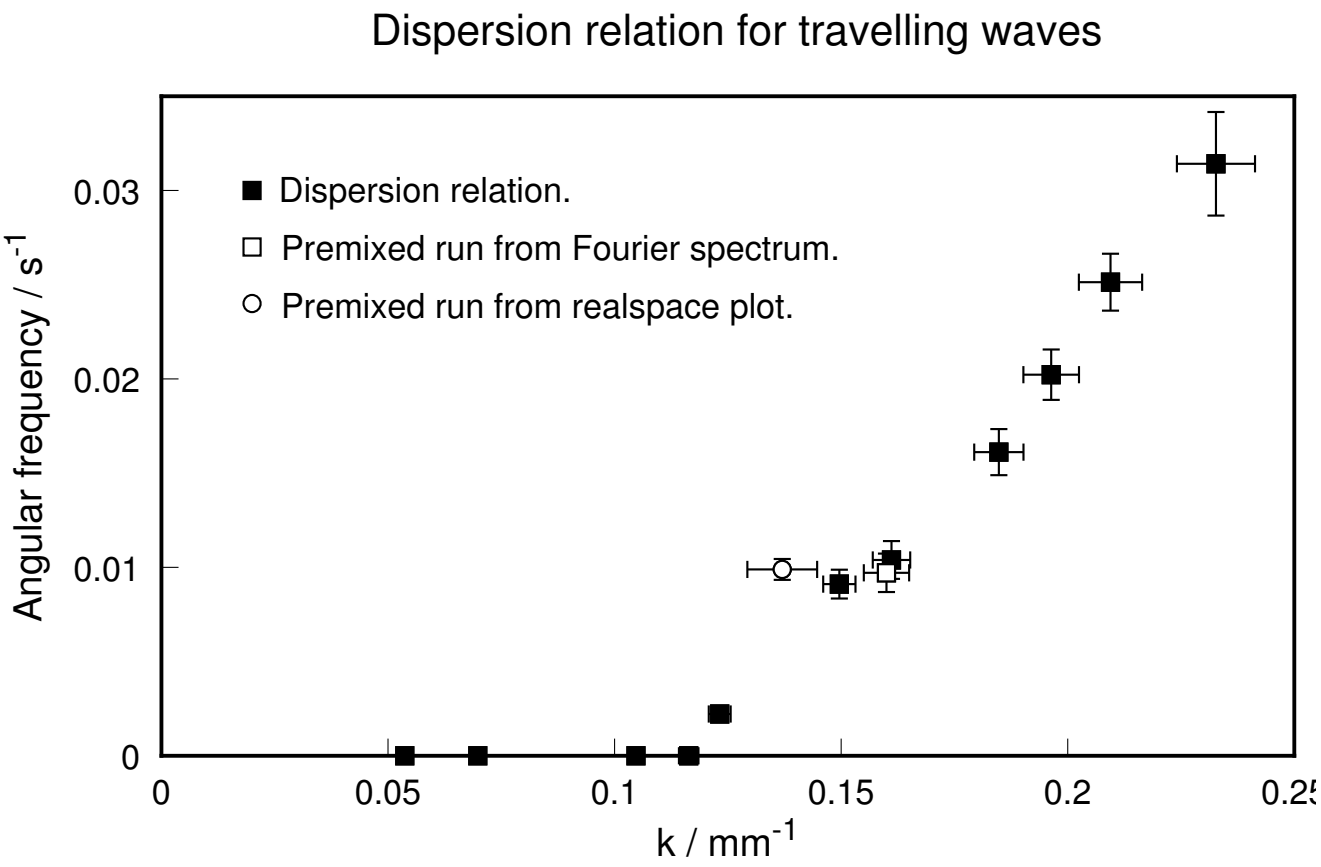

FIG. 14. Dispersion relation for travelling waves. $\omega = 4.841 s^{-1}$ and $\phi = 0.67$.

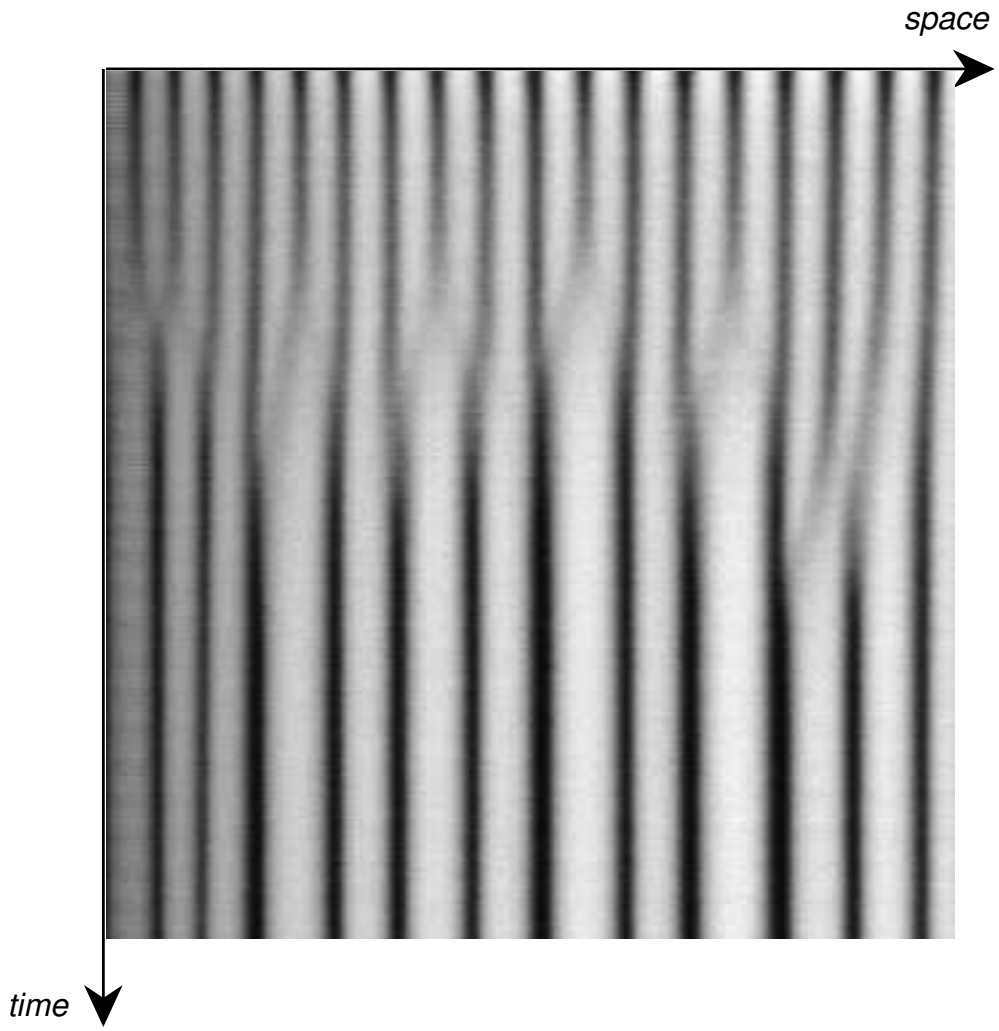

FIG. 15. Merging and frozen behaviour near the transition from travelling waves to frozen bands. $\omega = 4.841 s^{-1}$ and $\phi = 0.67$.

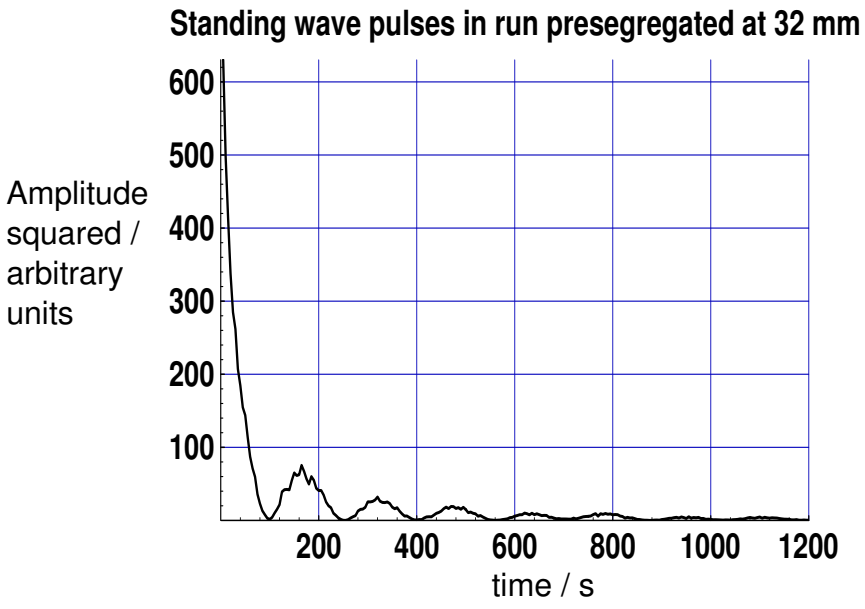

(a)

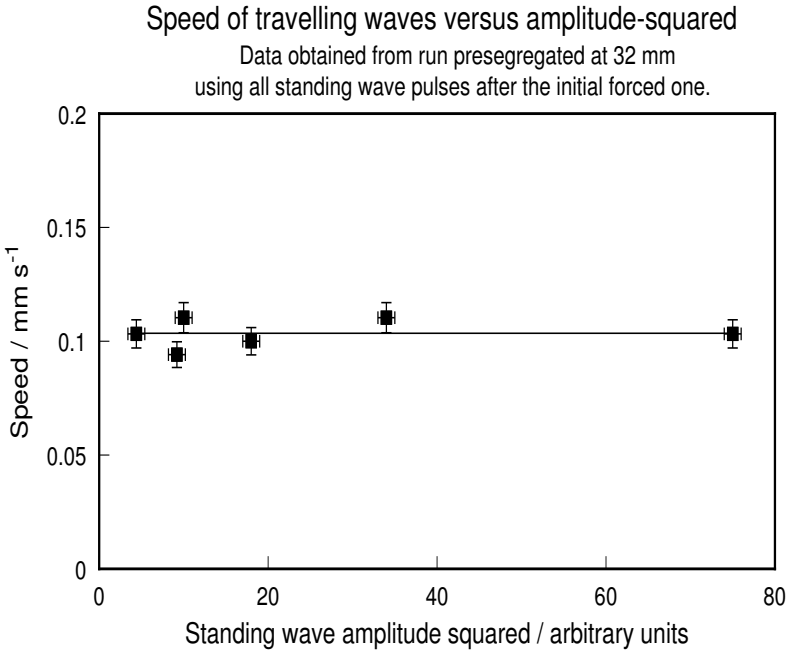

(b)

FIG. 16. (a) The amplitude of a standing wave damps away. (b) Plot of velocity derived from a standing wave pulse versus the amplitude-squared at the antinode of the pulse. Here, $\omega = 4.841 s^{-1}$ and $\phi = 0.67$.

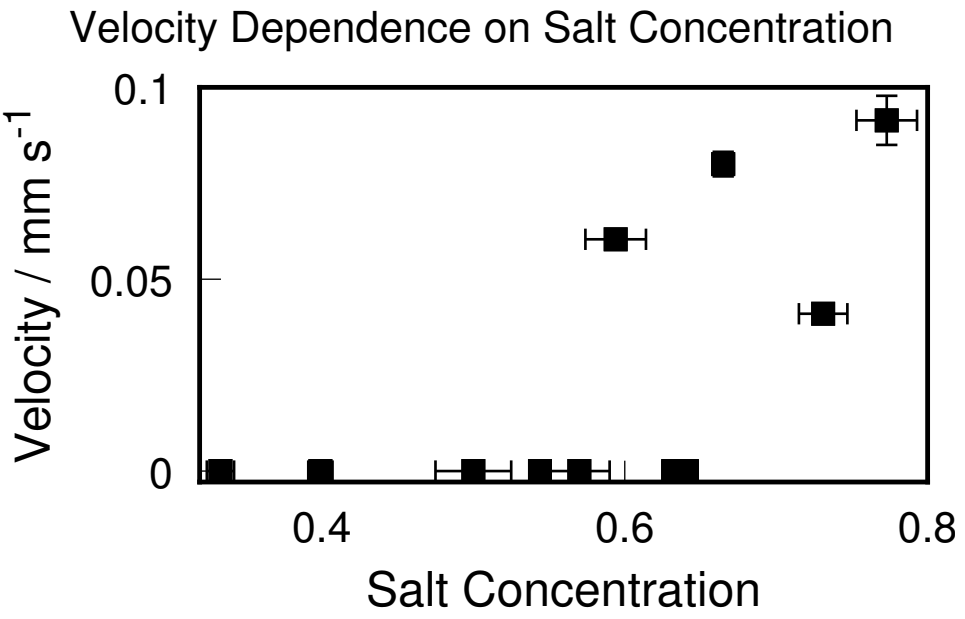

FIG. 17. Graph showing velocity dependence on mixture ratio for a fixed wavelength of 32 mm. $\omega = 4.841 s^{-1}$.

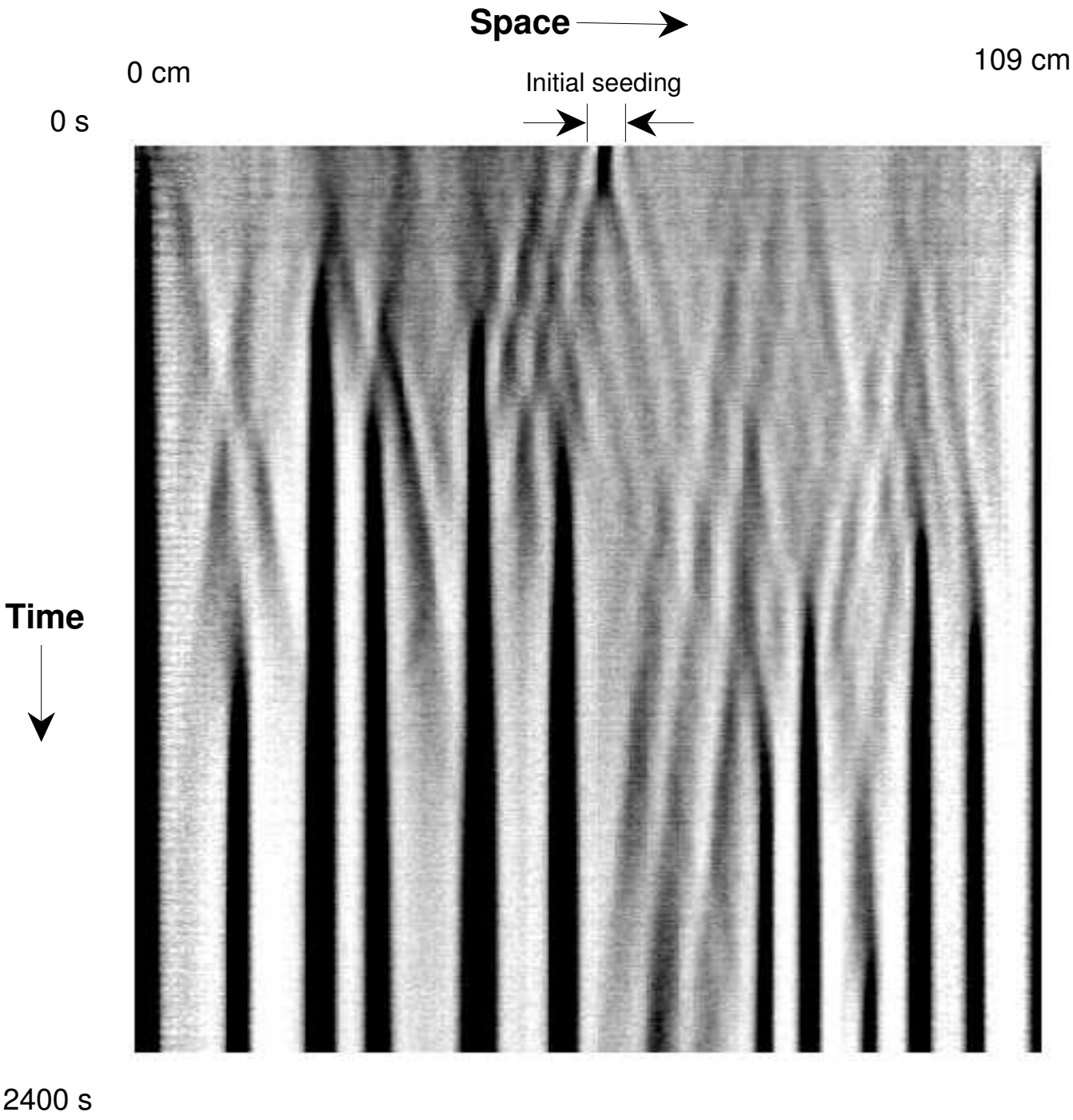

FIG. 18. Two pulses emerging from an initial condition that was premixed except at the centre, where a white-black-white seeding was laid down. The bands were of the same width: 10.6 mm.

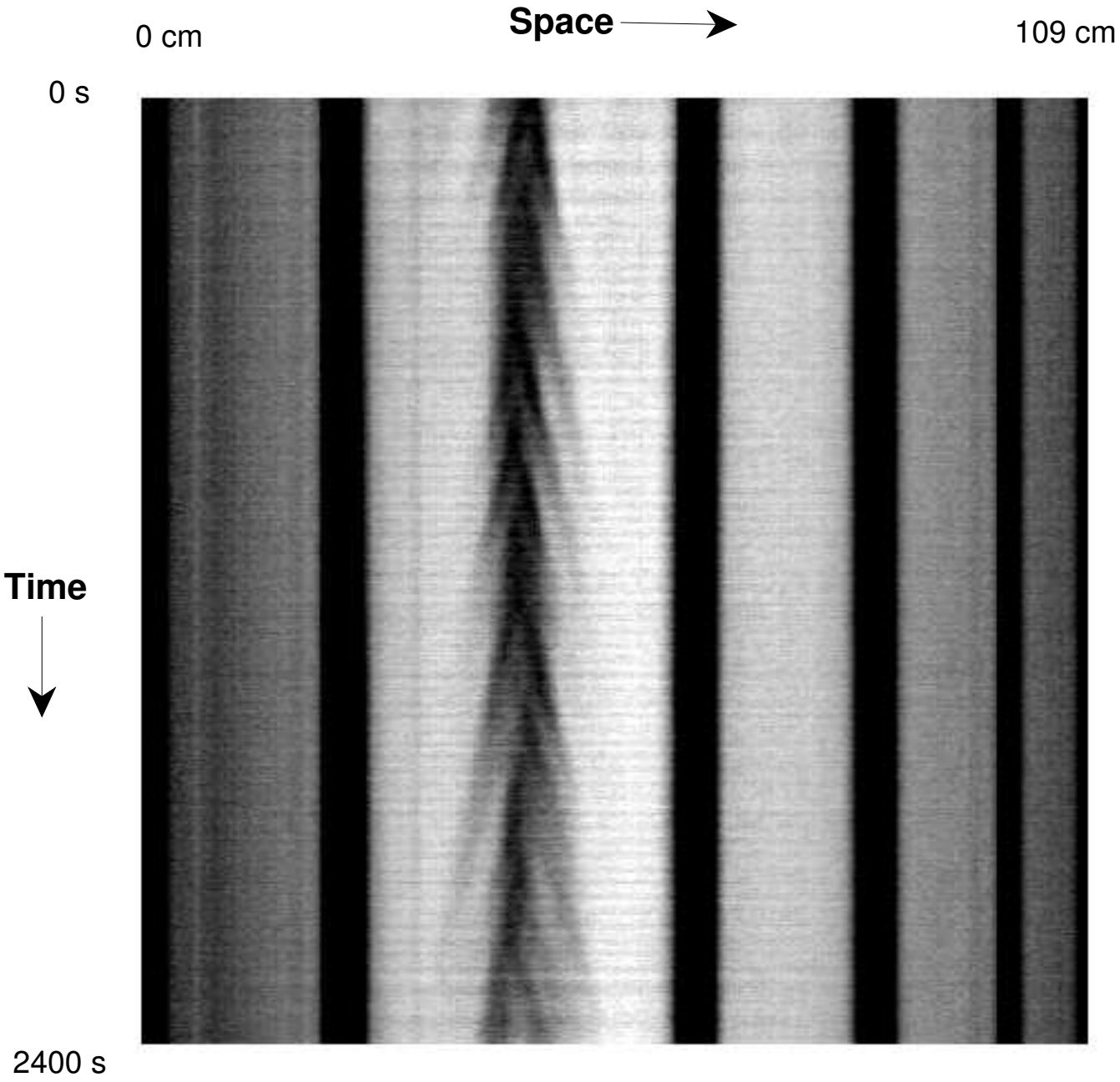

FIG. 19. A persistent source of waves that was stable over the duration of observation (40 minutes).

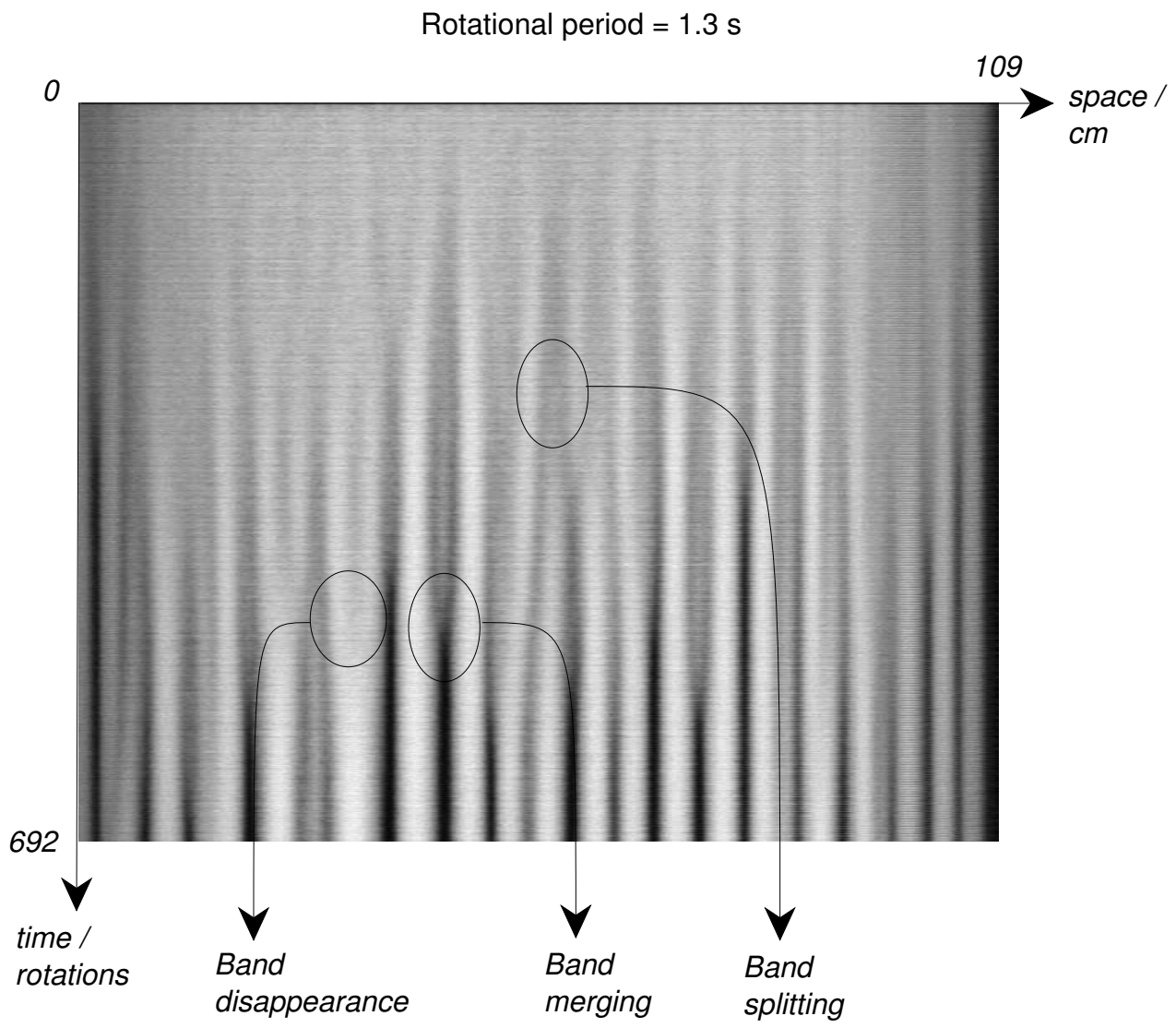

FIG. 20. An example showing band splitting, merging and disappearance.

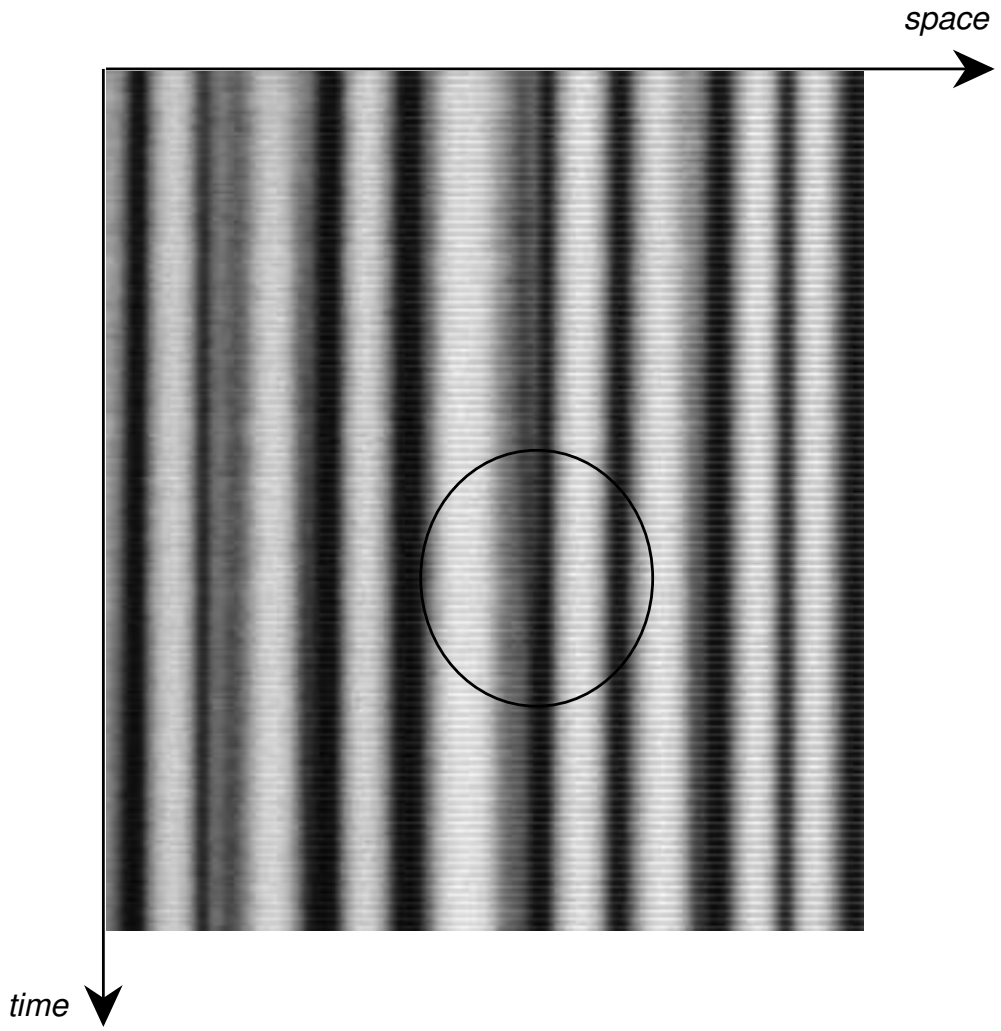

FIG. 21. An example showing an unsaturated band being absorbed by a saturated band.

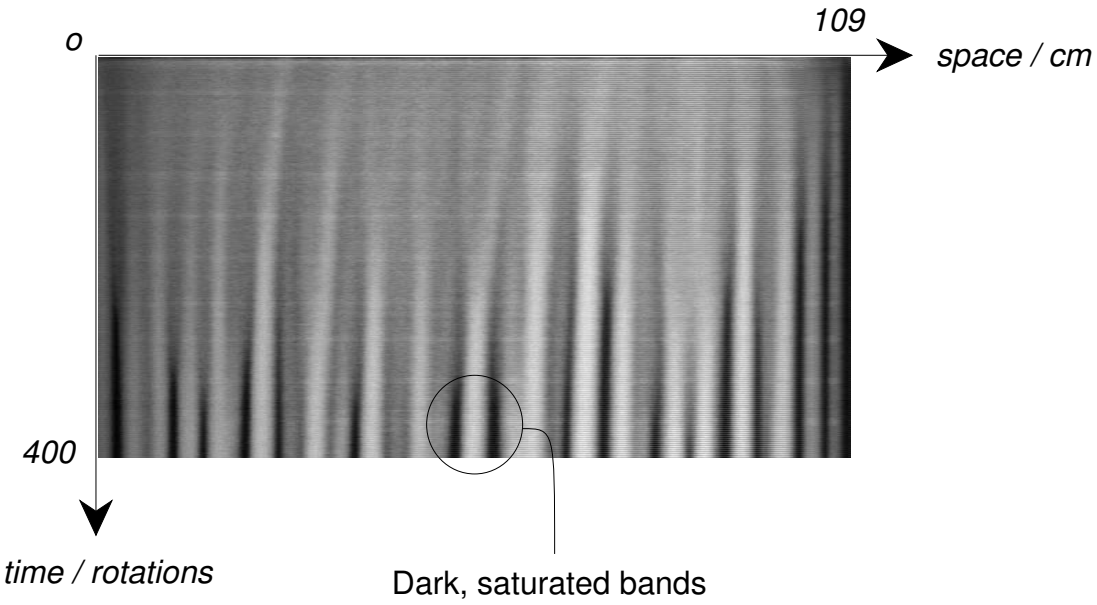

(a)

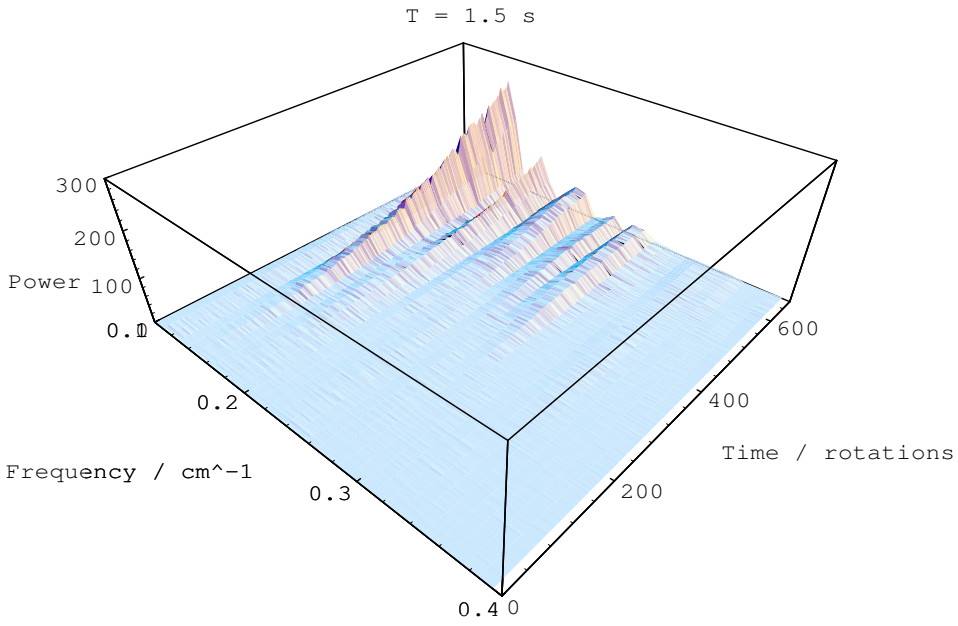

(b)

FIG. 22. (a) A typical run. (b) A 1D Fourier transform of a typical run. Here, $\omega = 4.19s^{-1}$.

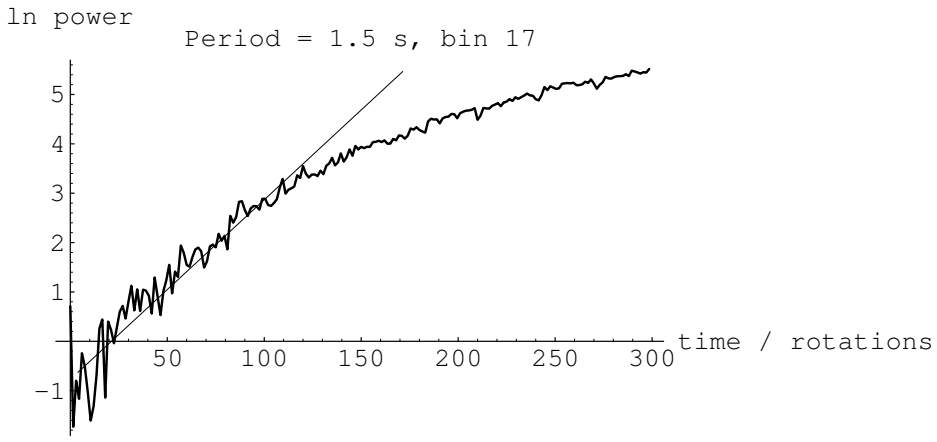

FIG. 23. Power growth in a single Fourier bin.

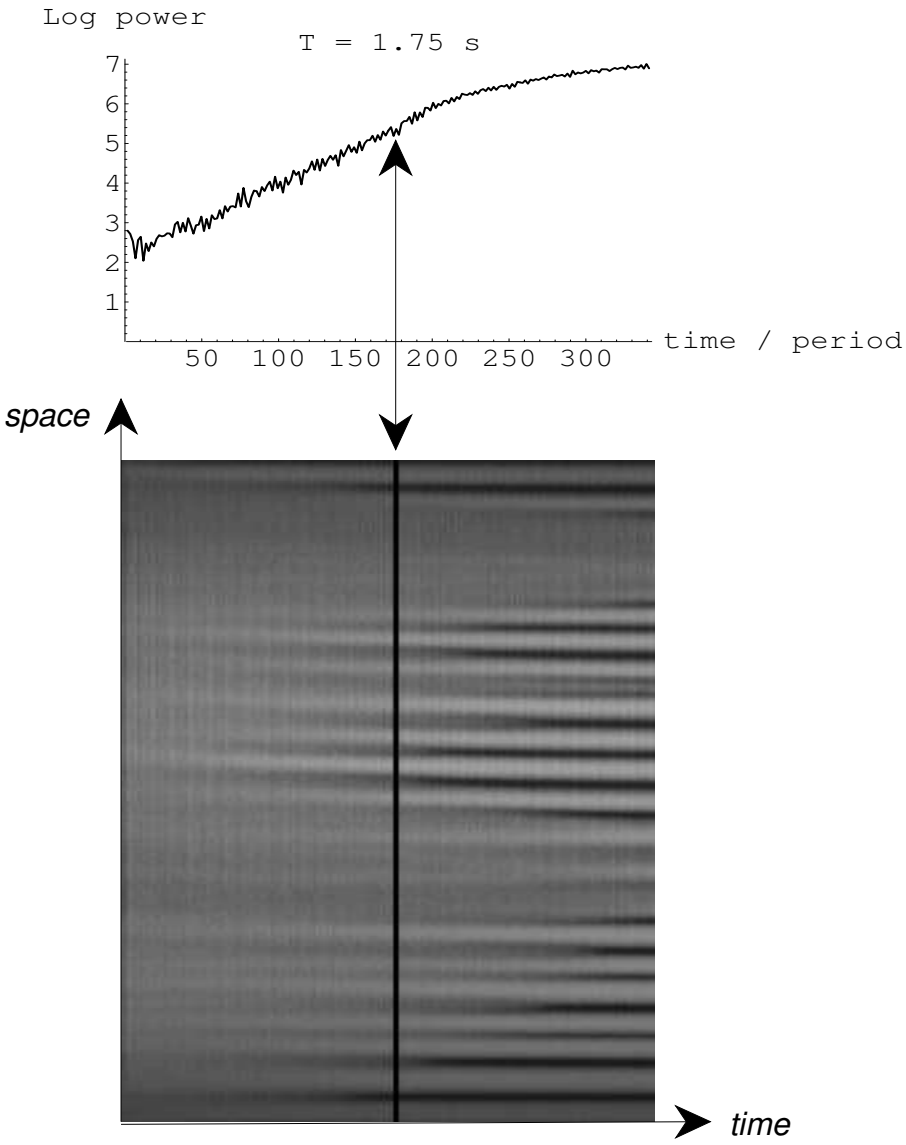

FIG. 24. Total power (less DC component) vs time, showing how loss of exponentiality corresponds to onset of saturation. Here $\omega = 3.59s^{-1}$.

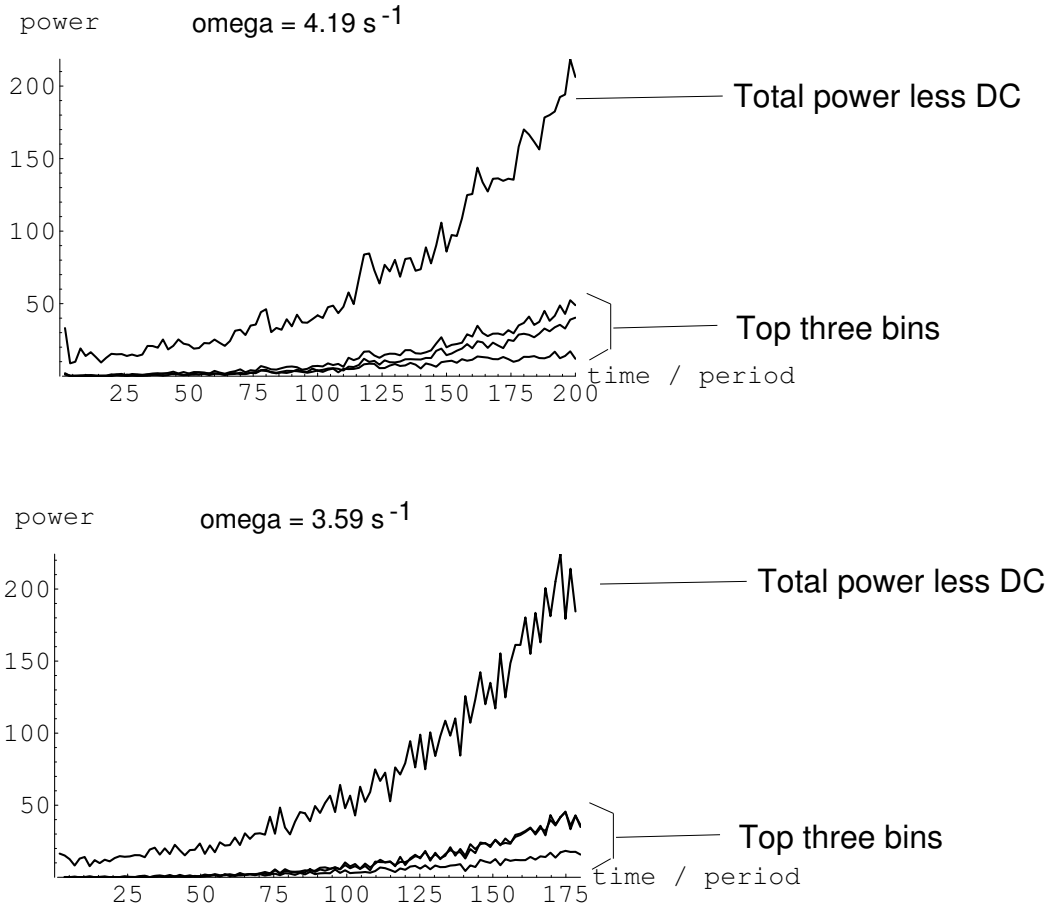

FIG. 25. Total power (less DC) compared to the top 3 Fourier modes.

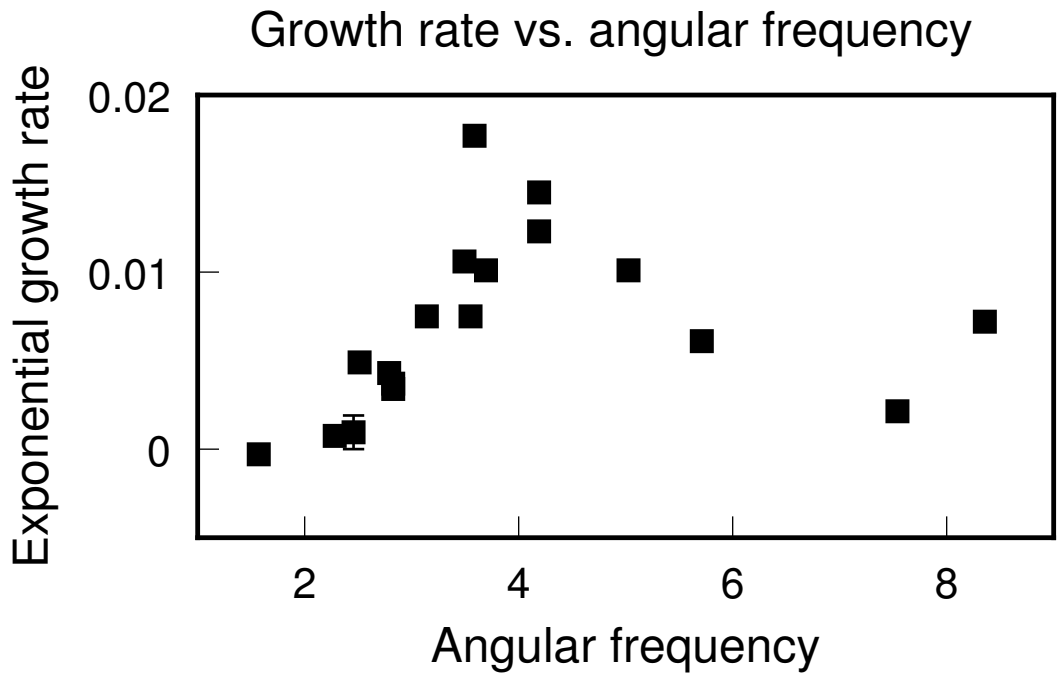

FIG. 26. Structural growth rate versus frequency. The structural growth rate is the exponential growth rate of the total Fourier power of the concentration, less the DC component.

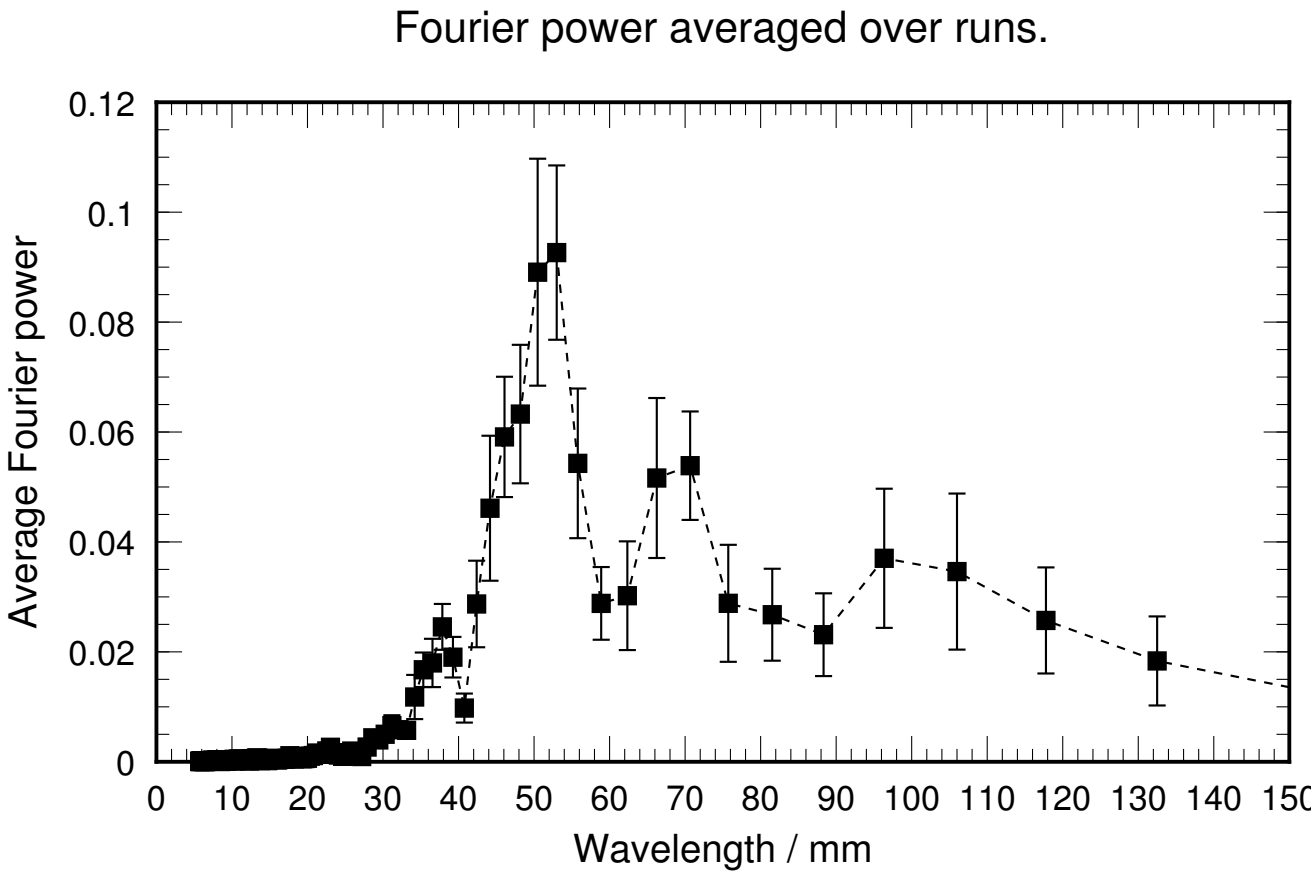

FIG. 27. Averaged Fourier spectrum showing one, possibly two peaks. Each spectrum is normalized by the total power outside DC. Then, all the spectra are added together to yield this average spectrum. The spectra were typically obtained at different ω's.

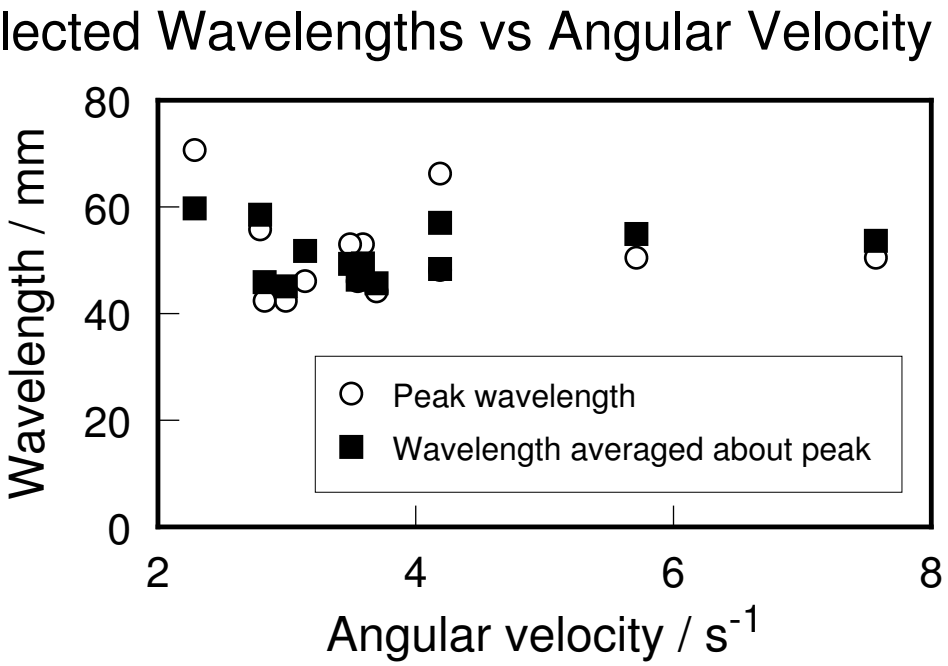

FIG. 28. Selected wavelength as a function of rotation rate. Hollow points represent the wavelength at which the largest peak occurs in the Fourier spectrum. Solid points represent the centre-of-mass wavelength obtained over Fourier bin 6 to twice the largest peak's bin. We begin averaging from bin 6 so as to avoid the DC component.

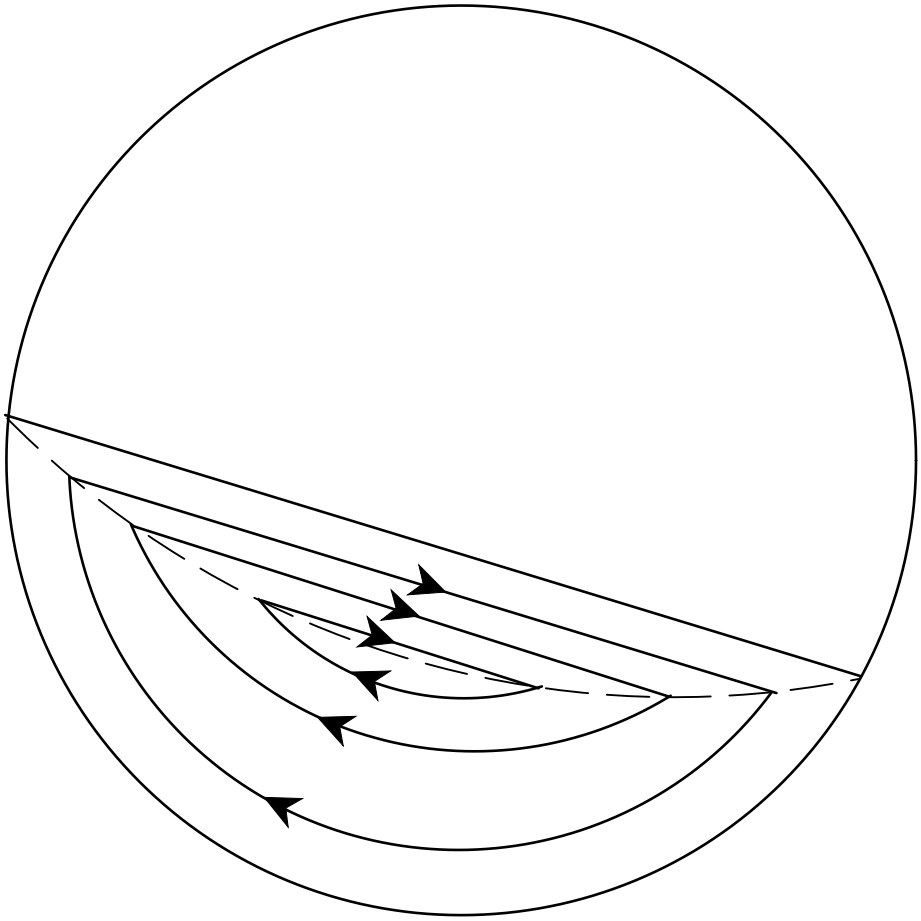

FIG. 29. Cross section of a tube showing the flowlines that tend to recur.

REFERENCES

[1] Y. Oyama, *Bull. Inst. Phys. Chem. Res. Rep.*, **5**, 600 (1939).

[2] M. C. Cross and P. C. Hohenberg *Rev. Mod. Phys.*, **65**, 851 (1993).

[3] A. C. Newell, *Spatio-Temporal Patterns in Nonequilibrium Complex Systems*, (Addison-Wesley Publishing Company, 1995), p 3.

[4] B. J. Ennis, *Powders et Grains 97*, (A. A. Balkema, 1997), p 13.

[5] H. M. Jaegar, S. R. Nagel and R. P. Behringer, *Rev. Mod. Phys.*, **68**, 1259 (1996).

[6] R. Chicharro, R. Peralta-Fabi, R. M. Velasco, *Powders et Grains 97*, (A. A. Balkema, 1997), p 479.

[7] O. Pouliquen, *Powders et Grains 97*, (A. A. Balkema, 1997), p 451.

[8] M. D. Shattuck, C. Bizon, P. B. Umbanhower, J. B. Swift and H. L. Swinney, (A. A. Balkema, 1997), p 429, and references therein.

[9] M. D. Shattuck, private communication.

[10] H. M. Jeager and S. R. Nagel, *Science*, **255**, 1523 (1992).

[11] J. Bridgwater, *Powder Technol.*, **15**, 215 (1976).

[12] M. B. Donald and B. Roseman, *British Chem. Eng.*, **7**, 749 (1962).

[13] S. Das Gupta, D. V. Khakhar and S. K. Bhatia, *Chem. Eng. Sci.*, **46**, 1513 (1991).

[14] S. B. Savage, *Disorder and Granular Media*, D. Bideau and A. Hansen, ed. (North Holland, Amsterdam, 1993), p. 255.

[15] M. Nakagawa, *Chem. Eng. Sci.*, **49**, 2540 (1994).

[16] M. Nakagawa, S. A. Altobelli, A. Caprihan, E. Fukushima, E. K. Jeong, *Experiments in Fluids*, **16**, 54 (1993).

[17] O. Zik, D. Levine, S. G. Lipson, S. Shtrikman and J. Stavans, *Phys Rev. Lett.*, **73**, 644 (1994).

[18] K. M. Hill and J. Kakalios, *Phys. Rev. E*, **49**, R3610 (1994), and **52**, 4393 (1995).

[19] K. M. Hill, A. Caprihan and J. Kakalios, *Phys Rev. Lett.*, **78**, 50 (1997).

[20] K. L. Gavrilov, *Powders et Grains 97*, (A. A. Balkema, 1997), p 523, and references therein.

[21] D. V. Khakhar, J. J. McCarthy, Troy Shinbrot and J. M. Ottino, *Phys. Fluids*, **9**, 31 (1997).

[22] E. Clement, J. Rajchenbach and J. Duran, *Europhysics Letters*, **30**, 7 (1995).

[23] F. Melo, P. Umbanhower, H. L. Swinney, *Phys. Rev. Lett.*, **72**, 172 (1994), and **75**, 3838 (1995).

[24] K. M. Aoki, T. Akiyama, Y. Maki, T. Watanabe, *Phys. Rev. E*, **54**, 874 (1996).

[25] S. Douady, S. Fauve, C. Laroche, *Europhys. Lett.*, **8**, 621 (1989).

[26] S. Fauve, C. Laroche and S. Douady, *Physics of Granular Media*, (Nova Science Publishers, Commack, N.Y., 1991) p. 277.

[27] "Scenic Sand", manufactured by Activa Products Inc., P.O. Box 1296, Marshall, TX, 75670.

[28] W. van Sarloos, *Spatio-Temporal Patterns*, (Addison-Wesley, 1995) p 19.

[29] P. Kolodner, *Phys. Rev. Lett.*, **66** 1168, (1991), and references therein.